MINISTRY OF DEFENCE (AVIATION SUPPLY)

AERONAUTICAL RESEARCH COUNCIL
REPORTS AND MEMORANDA

Turbulent Boundary Layers on a Large Flat Plate at $M = 4$

by R. C. HASTINGS and W. G. SAWYER

Aerodynamics Dept., RAE, Bedford

LONDON: HER MAJESTY'S STATIONERY OFFICE
1971
PRICE £2·10 NET

Turbulent Boundary Layers on a Large Flat Plate at $M = 4$

By R. C. HASTINGS and W. G. SAWYER

Aerodynamics Dept., RAE, Bedford

Reports and Memoranda No. 3678*
March, 1970

Summary.

Transition positions, local skin-friction coefficients and boundary layer profiles measured in adiabatic flow on a flat plate are given. The data are for turbulent flow and cover a range of momentum-thickness Reynolds numbers of approximately 2500 to 25000. At high Reynolds number, skin-friction coefficients are well predicted by the relations of Spalding and Chi or Winter and Gaudet. Below a Reynolds number of roughly 10000 the results, though less reliable, seem to lie above these predictions; the higher values are corroborated by data from other sources.

The inner parts of the velocity profiles follow a common law, well predicted by the correlation of Winter and Gaudet, and at high Reynolds numbers the velocity-defect profile of the outer layer agrees with a number of previous predictions. The outer parts of the profiles exhibit a wake component which decreases with decreasing Reynolds number and eventually vanishes. In respect of this behaviour, the compressible flow corresponds to an incompressible flow at a much lower Reynolds number.

*Replaces RAE Tech. Report No. 70040—A.R.C. 32 427.

LIST OF CONTENTS

1. *Introduction.*

The behaviour of turbulent boundary layers in compressible flow is a topic of considerable practical importance, and one for which there is no exact theory. Consequently, experimental data are continually needed to enable semi-empirical theories to be formulated and tested. This Report gives a set of measurements made for these purposes. The measurements were made in the boundary layer of a large, flat plate, to which heat transfer was small, immersed in an airstream at a Mach number of 4. The main results consist of velocity profiles and skin-friction measurements. Positions of natural transition from laminar to turbulent flow are also given.

In order to provide a framework within which to discuss the measurements, some boundary-layer theories are briefly described. The skin-friction laws of these theories are compared with the measurements in terms of relations between skin-friction coefficient and Reynolds number based on momentum thickness. Because there were clear indications that the flow along the centre-line of the plate was slightly convergent, no comparisons are made in terms of skin friction as a function of length Reynolds number.

To provide a further comparison with theory, the forms of the measured velocity profiles in the wall region and the outer, 'velocity-defect' region are examined.

2. *Theories for Predicting Skin Friction.*

2.1. *General Background.*

For a fluid with velocity u, density ρ, viscosity μ and shear stress τ, and using the suffices w and e to denote conditions respectively at the wall and in the flow external to the boundary layer, we make the following definitions:

$$\left.\begin{aligned} &\text{local skin-friction coefficient,} && C_f = \frac{2\tau_w}{\rho_e u_e^2}, \\ &\text{unit Reynolds number,} && R = \frac{\rho_e u_e}{\mu_e}, \\ &\text{boundary-layer momentum thickness,} && \delta_2 = \int_0^\infty \frac{\rho u}{\rho_e u_e}\left(1-\frac{u}{u_e}\right) dy, \end{aligned}\right\} \quad (1)$$

where y is distance normal to the wall.

We then adopt the convention of regarding the various theories for skin friction in compressible flow as statements of a supposed correspondence between the actual flow (without suffix) and a related incompressible flow (suffix i). The correspondence is defined by:

$$\left.\begin{aligned} C_{fi} &= F_c C_f \ , \\ R_i x_i &= F_x R x \ , \\ R_i \delta_{2i} &= F_\delta R \delta_2 , \end{aligned}\right\} \quad (2)$$

where x is the distance downstream from the virtual origin of the boundary layer. The compressibility factors F_c, F_x and F_δ are in general functions of Mach number M_e, the temperatures at the wall, T_w, and in the freestream, T_e, and Reynolds number.

Because there is no universally accepted theory for turbulent boundary layers, neither are there agreed values for F_c, F_x and F_δ. Indeed, since skin-friction coefficient is a smooth and monotonic function of Reynolds number, widely differing yet equally plausible compressibility factors are possible. This is easily illustrated by using the approximate incompressible law

$$C_{fi} = \frac{K}{(R_i x_i)^{\frac{1}{n}}} = \frac{L}{(R_i \delta_{2i})^{\frac{1}{n-1}}} \tag{3}$$

where K = constant

and $L = \left[\frac{n K^n}{2(n-1)}\right]^{\frac{1}{n-1}}$.

The relation between K and L is a consequence of the momentum equation

$$\frac{C_{fi}}{2} = \frac{d(R_i \delta_{2i})}{d(R_i x_i)}. \tag{4}$$

If F_c, F_x and F_δ are constants for a particular flow, it follows from (4) and the corresponding equation for compressible flow

$$\frac{C_f}{2} = \frac{d(R\delta_2)}{d(Rx)}, \tag{5}$$

that

$$F_c F_x = F_\delta, \tag{6}$$

whatever the functional form of the skin-friction law. Consequently the compressible law corresponding to (3) is

$$C_f = \frac{K}{F_c (F_x)^{\frac{1}{n}} (Rx)^{\frac{1}{n}}} = \frac{L}{F_c (F_\delta)^{\frac{1}{n-1}} (R\delta_2)^{\frac{1}{n-1}}}. \tag{7}$$

Thus any combination

$$F_c (F_x)^{\frac{1}{n}} = N = \text{constant}, \tag{8}$$

or alternatively

$$F_c (F_\delta)^{\frac{1}{n-1}} = N^{\frac{1}{n-1}}, \tag{9}$$

will yield the same compressible skin-friction law, i.e. however arbitrary the choice of F_x or F_δ, the same law will result if F_c is then chosen to fit a given set of experimental data. Since in most methods the scaling factors are derived empirically, or at least the factors proposed are justified by comparison with experiment, it is difficult to make a critical assessment of the various theories simply by further comparisons with experimental values of skin friction.

Application of most methods to adiabatic flow leads to $F_c > 1$; F_x, $F_\delta < 1$; that is to say, a compressible flow corresponds to an incompressible flow at lower Reynolds number. It seems intuitively reasonable that this should be so, since it is generally accepted that viscosity plays an important part only in the region close to the wall. With increasing Mach number the static temperature at the wall increases relative to that outside the boundary layer, the kinematic viscosity (which varies across the layer roughly as the square of temperature) increases also, and there is therefore a relative reduction in the local unit Reynolds number close to the wall.

2.2. *Particular Methods.*

2.2.1. *Intermediate-temperature methods.* It is supposed that, if fluid density and viscosity are evaluated at some temperature T' intermediate between the temperature of the wall T_w and that of the external stream T_e, then a single relation for skin friction may be used in both compressible and incompressible flow. If, for incompressible flow, this relation is written:

$$\frac{2\tau_{wi}}{\rho_{ei}\, u_{ei}^2} = C_{fi} = \phi_1\left[\frac{\rho_i\, u_{ei}\, x_i}{\mu_i}\right], \tag{10}$$

then, for compressible flow, it becomes

$$\frac{2\tau_w}{\rho'\, u_e^2} = C_f' = \phi_1\left[\frac{\rho'\, u_e\, x}{\mu'}\right]. \tag{11}$$

Since T' occurs part way across the boundary layer and static pressure is constant,

$$\rho'\, T' = \rho_e\, T_e \tag{12}$$

for a perfect gas.
The compressibility factors of equation (2) are thus

$$\left.\begin{aligned} F_c &= \frac{T'}{T_e}, \\ F_x &= \frac{\mu_e\, T_e}{\mu'\, T'} \\ &\text{and hence, from (6),} \\ F_\delta &= \frac{\mu_e}{\mu'}. \end{aligned}\right\} \tag{13}$$

Well known formulae for intermediate temperature are:

$$\frac{T'}{T_e} = 1+0{\cdot}5\left(\frac{T_w}{T_e}-1\right)+0{\cdot}22\left(\frac{T_r}{T_e}-1\right); \tag{14}$$

i.e.

$$\frac{T'}{T_e} = 1+0{\cdot}5\left(\frac{T_w}{T_e}-1\right)+0{\cdot}22\left(\frac{\gamma-1}{2}\right) r\, M_e^2,$$

where

$$\frac{T_r}{T_e} = 1+r\left(\frac{\gamma-1}{2}\right) M_e^2. \tag{15}$$

Alternatively

$$\frac{T'}{T_e} = 1+0{\cdot}45\left(\frac{T_w}{T_e}-1\right)+0{\cdot}035\, M_e^2. \tag{16}$$

Equation (14) was given by Eckert[1] and equation (16) by Sommer and Short[2]. In equation (15) r is the recovery factor, taken here to be 0·89; γ is the ratio of specific heats for the gas, taken here to be 1·4 for air; and M_e is the Mach number of the external stream. For adiabatic flow ($T_w = T_r$) the respective intermediate temperatures are:

$$\text{Eckert;} \qquad \frac{T'}{T_e} = 1 + 0{\cdot}128\, M_e^2 \tag{17}$$

$$\text{Sommer and Short;} \qquad \frac{T'}{T_e} = 1 + 0{\cdot}115\, M_e^2 . \tag{18}$$

2.2.2. *Transformation methods.* There have been several attempts to derive transformations relating the differential equations of mean motion in turbulent compressible and incompressible flows. The goal of such transformations is to enable treatments which are well established for incompressible flow to be carried over to deal with compressible flows. It is well known that for laminar flow a complete formal transformation exists between compressible and incompressible flows at constant pressure, provided that the gas is of Prandtl number unity and has viscosity proportional to temperature. Under the transformation the velocity ratio u/u_e is invariant and the ordinate $\bar{y}$ satisfies the condition $d\bar{y} \sim \rho\, dy$. Consequently the momentum thickness transforms immediately to incompressible form:

$$\delta_2 = \int_0^\infty \frac{\rho u}{\rho_e u_e}\left(1 - \frac{u}{u_e}\right) dy$$

$$= \lambda \int_0^{\bar{y}} \frac{u}{u_e}\left(1 - \frac{u}{u_e}\right) d\bar{y}$$

where $\bar{y} = \dfrac{1}{\lambda}\displaystyle\int_0^y \frac{\rho}{\rho_e}\, dy$ and λ is a scaling factor.

Transformations proposed for turbulent flow have usually been linked to intermediate temperature methods; for example, Spence[3] presented evidence showing the utility of the transformed ordinate $y = \displaystyle\int_0^y \frac{\rho}{\rho'}\, dy$, where ρ' was evaluated at Eckert's intermediate temperature of equations (14) and (17).

Since then, Coles[4] has discussed transformation theory in considerable detail in a paper whose main purpose is to expound a new transformation involving scaling factors which are Reynolds-number dependent. To be compatible with each other at the wall, corresponding stations in related flows have to satisfy the relation

$$C_f R\delta_2 = \frac{\mu_w \rho_w}{\mu_e \rho_e} C_{fi} R\delta_{2i},$$

which Coles terms the 'Law of Corresponding Stations'. Momentum-thickness Reynolds numbers are related by:

$$R\delta_2 = \frac{u_s}{u_e} R_i \delta_{2i},$$

where μ_s is the viscosity at a sub-layer temperature T_s. This sub-layer temperature, derived empirically, is given by:

$$\frac{T_s}{T_e} = 1 + (1 - 0{\cdot}544\, c)\left(\frac{T_w}{T_e} - 1\right) + c\,(0{\cdot}544 - 0{\cdot}305\, c)\left(\frac{\gamma - 1}{2}\right) M_e^2, \tag{19}$$

$$\text{where } c = \left(\frac{10^3\, C_{fi}}{2}\right)^{\frac{1}{2}}.$$

At practical Reynolds number c is of order unity; it does however vary quite rapidly at low Reynolds number. Consequently (19), though resembling (14) and (16), often yields rather different results. Compressibility factors for Coles' method are:

$$F_c = \frac{T_w}{T_e}\frac{\mu_s}{\mu_w}$$

and

$$F_\delta = \frac{\mu_e}{\mu_s} \tag{20}$$

2.2.3. *Van Driest's mixing-length method.* Van Driest[5], extending the mixing-length arguments first put forward by Prandtl[6], derived a skin-friction relation which for compressible flow is written:

$$\frac{1}{(C_f)^{\frac{1}{2}}}\left[\frac{\sin^{-1}\alpha + \sin^{-1}\beta}{\bar{A}\,(T_w/T_e)^{\frac{1}{2}}}\right] = 1{\cdot}694 + 4{\cdot}132 \log_{10}\left[\frac{Rx\, C_f}{(T_w/T_e)^{\omega}}\right] \tag{21}$$

$$\text{where } \bar{A}^2 = \frac{T_e}{T_w}\left(\frac{\gamma - 1}{2}\right) M_e^2\ ;\quad \bar{B} = \frac{T_e}{T_w}\left(1 + \left(\frac{\gamma - 1}{2}\right) M_e^2\right) - 1\ ;$$

$$\alpha = \frac{2\bar{A}^2 - \bar{B}}{(\bar{B}^2 + 4\bar{A}^2)^{\frac{1}{2}}} \quad ;\quad \beta = \frac{\bar{B}}{(\bar{B}^2 + 4\bar{A}^2)^{\frac{1}{2}}}\ ;$$

and the viscosity law is taken to be $\mu \sim T^{\omega}$.
In incompressible flow, equation (21) reduces to:

$$\frac{1}{(C_{fi})^{\frac{1}{2}}} = 1{\cdot}694 + 4{\cdot}132 \log_{10}\left[R_i\, x_i\, C_{fi}\right]. \tag{22}$$

Using the definitions (2) and equation (6) we find from (21) and (22) that the scaling factors are:

$$F_c = \frac{T_w\, \bar{A}^2}{T_e\,(\sin^{-1}\alpha + \sin^{-1}\beta)^2},$$

$$F_x = \frac{(\sin^{-1}\alpha + \sin^{-1}\beta)^2}{\bar{A}^2} \cdot \left(\frac{T_e}{T_w}\right)^{1+\omega} \tag{23}$$

and

$$F_\delta = \left(\frac{T_e}{T_w}\right)^{\omega} = \frac{\mu_e}{\mu_w}.$$

2.2.4. *The method of Spalding and Chi.* These authors, in a review[7] of the then existing theories for skin friction, concluded from extensive comparisons with experiment that mixing-length theories were the most successful. They went on from this to develop an empirical theory of their own, taking as a starting point F_c to be defined in equation (23) but with $r\left(\frac{\gamma-1}{2}\right)M_e^2$ substituted for $\left(\frac{\gamma-1}{2}\right)M_e^2$ in van Driest's expressions for $\bar{A}$, $\bar{B}$, α and β. Recovery factor was taken as 0·89 and F_δ was chosen empirically, from a least-squares fit to the available data, as:

$$F_\delta = \left(\frac{T_e}{T_w}\right)^{0\cdot702}\left(\frac{T_r}{T_w}\right)^{0\cdot772} \tag{24}$$

For adiabatic flow the method gives similar results to intermediate temperature theory. In flows with appreciable heat transfer, however, the variation of skin friction with heat transfer is, according to Spalding and Chi, considerably less than that predicted by earlier theories.

The empirical development of the method can be criticised on the grounds that it was based on experimental data of very uneven quality, and that too much reliance was placed on the viscosity law $\mu \sim T^{0\cdot76}$. This approximation is not very accurate for wind-tunnel conditions. Nevertheless, subsequent work has tended to confirm the value of the Spalding and Chi method as an engineering tool.

2.2.5. *The method of Winter and Gaudet.* Winter and Gaudet[8], in an extension of previous work[9], have recently presented a correlation based on the observation that the shape of the velocity profile does not vary perceptibly when Mach number is varied with Reynolds number (based on some characteristic overall scale of the boundary layer) held constant. They have found that skin friction in adiabatic flow can usefully be expressed as a function of Reynolds number based on a kinematic integral* analogous to momentum thickness:

$$F_c C_f = \phi_2\left[R\delta_2{}^{(u)}\right]$$

where

$$\delta_2{}^{(u)} = \int_0^\infty \frac{u}{u_e}\left(1-\frac{u}{u_e}\right)dy \tag{25}$$

It follows immediately that

$$F_\delta = \frac{\delta_2{}^{(u)}}{\delta_2}$$

and for this Winter and Gaudet[8] derived the empirical relation

$$F_\delta = 1+0\cdot056\,M_e^2\,. \tag{26a}$$

At the same time it was found that a suitable empirical form for F_c was

$$F_c = \left(1+\frac{\gamma-1}{2}M_e^2\right)^{\frac{1}{2}} \tag{26b}$$

*Winter and Gaudet[8] denote these integrals by the superscript i, but, to avoid confusion with the present notation of equation (2), the superscript u is used in this Report.

and so, from (6),

$$F_x = \frac{1+0{\cdot}056\,M_e^2}{(1+0{\cdot}2\,M_e^2)^{\frac{1}{2}}}. \tag{26c}$$

It is interesting to note that the correlation of Winter and Gaudet differs from all others in having $F_\delta > 1$.

2.2.6. *General calculation procedures.* Recently a number of authors have proposed that boundary-layer development in flows with pressure gradients may be calculated using finite difference methods to solve a set of partial differential equations which includes, explicitly or implicitly, a modelling of the turbulence structure. In applying such methods to compressible flow, the authors commonly assume that their model of the turbulence structure is not influenced by compressibility. It is then possible to use the method, as Bradshaw and Ferriss[10] have done, to compute constant-pressure flows at various Mach numbers. From such computations we could, of course, determine the relation between C_f and $R\delta_2$. Bradshaw and Ferriss illustrate their method by presenting example velocity profiles at Mach numbers of 0, 1, 2·2, 3 and 4. For these illustrative examples, computed skin-friction coefficients are within 2·5 per cent of the predictions of Spalding and Chi.

2.3. *Comparison of Methods.*

A selection of skin-friction relations for adiabatic flow at $M = 4$ is shown in Fig. 1. Although some of the difference between these relations arises because they are based on different skin-friction relations for incompressible flow, the major source of discrepancy is the choice of the factors F_c, F_x and F_δ. Compressibility factors for all the methods discussed earlier, except the last for which none are given, are compared in Table 1. True viscosity for this table was obtained from Sutherland's law, written

$$\mu = 3{\cdot}045 \times 10^{-8}\ \frac{T^{3/2}}{T+110{\cdot}4}\ \text{slug/ft sec at } T°K\,.$$

In the temperature range appropriate to wind-tunnel flow the exponent ω in a power viscosity law is rather higher at free-stream temperature than at wall temperature. The effect of different viscosity assumptions on the relation proposed by van Driest is included in Table 1.

The table includes two extra quantities. The first is the product $F_c\,F_\delta$ which, for ω unity, would be unity in an intermediate temperature method, and which for transformations is equal to $\mu_e\,\rho_e/\mu_\omega\,\rho_\omega$ according to Coles' 'Law of Corresponding Stations'. The last column gives $F_c\,(F_\delta)^{\frac{1}{n-1}}$ with n taken as 5; according to the arguments of Section 2.1, this quantity should not vary much between methods.

3. *Description of Experiment.*

3.1. *Wind Tunnel and Model Mounting.*

The tests were performed in the 3ft by 4ft supersonic tunnel at R.A.E. Bedford. This is a continuous tunnel fitted, at the time of the tests, with a wooden nozzle producing a Mach number of approximately four. Models to be tested in the tunnel are mounted so as to protrude forward from a model-support section which is wheeled up on a railway to the downstream end of the nozzle. The flat plate on which the present measurements were made was mounted, working face downwards, from the underside of support arms screwed to the sides of a model-support section.

3.2. *Model.*

Since the model, illustrated in Fig. 2, had to enter the nozzle as described above, its span was limited to 35 inches to provide a half inch clearance from the nozzle walls on each side. It consisted of a mild-steel plate, with a centre-line chord of 65 inches, having its working (lower) surface ground smooth to within 25μinches. The leading edge was chamfered on the upper side at 10 degrees included angle to a

nose of thickness 0·01 inch. Downstream of the chamfer the upper surface of the plate was ground, over the central third of its span, to be flat and parallel with the working surface so as to provide an instrumentation platform. The main instrumentation stations were twenty two holes, 1·625 inches in diameter, arranged along the centre line of the plate in alternate staggered rows of three and two.
This arrangement provides four identical groups of five holes followed by a final downstream pair. The holes could be filled with instrumented plugs whose faces were flush with the plate surface to within 0·0005 inch.

3.3. *Instrumentation.*

The main instruments—traversing probes, skin-friction meter and surface pitot-tubes—are described in separate sub-sections. Pressures and temperatures were measured and recorded in the following ways.

Surface pitot pressures and associated static pressures were measured by a Statham PA 208 TC-350 transducer having a range of 0–10 inches *Hg* absolute. It was used in conjunction with a Scanivalve 48D stepping switch, operated with alternate ports connected to vacuum to ensure that all measured pressures were approached from below.

Traverse probe pressures were measured by a C.E.C. 4–312 differential transducer of range ± 10 inch *Hg*. One side of this transducer was connected to a reference tank whose pressure, which was controllable, was monitored by a Midwood 0–60 inch *Hg*, servo-balanced, capsule and weighbeam manometer.

Copper-constantan thermocouples with beads of about 0·01 inch diameter were used to measure all temperatures. Their reference junctions were enclosed in a chamber immersed in a water bath in which the temperature was controlled and measured to an accuracy of $\pm 0{\cdot}1°C$.

Thermocouple and pressure-transducer voltages were fed to Speedomax G recorders which, like the Midwood manometer, were fitted with shaft encoders supplying digital information to punched cards.

3.3.1. *Pitot traverse gear.* Two identical, electrically driven traverse mechanisms were used. The associated pitot probes had round tips both with outside diameters of 0·014 inch but with different internal diameters. One, which was used at stations 2·5 inches to the port side of the centre line and at distances of 42, 32 and 22 inches from the leading edge, had an internal diameter of 0·011 inch. The other, used at stations 2·5 inches to starboard of the centre line and 46, 36, 26 and 16 inches from the leading edge, had an internal diameter of 0·005 inch.

A traverse mechanism and an enlarged view of a probe head are illustrated in Fig. 3. As shown, each pitot-tube contained a thermocouple bead. The temperature of this bead was recorded while air was being sucked through the probe at a rate sufficient to choke its entry. Pressure measurements were made during separate runs.

A twelve-step transmitter gave pitot stem movement with a resolution of 0·0001 inch from a datum determined by electrical contact between the tip of the probe and the surface of the instrumented plug.

3.3.2. *Floating-element skin-friction meter.* The skin-friction meter is illustrated in Fig. 4. The element was circular and had a diameter of 0·312 inch. The thickness of its edge was kept to a minimum (0·01 inch) to ensure that the chordwise force arising from any streamwise pressure gradients would be small. Static-pressure tappings were not provided in the housing around the element to sense any pressure forces on it, because there was not sufficient space available. The average gap around the element was 0·005 inch. The element was supported by encastré leaf springs and allowed to move under load. Its movement was measured by a Schaevitz linear variable differential transformer energised by 3 volts at 5 kHz. Vibration of the element was heavily damped by vanes moving in dashpots of 100 centistoke silicone oil. To calibrate the meter, weights were placed in a scale pan, hanging on a thread which passed over a pulley mounted on jewel bearings, to apply a tangential force to the element.

3.3.3. *Surface static and pitot pressures.* As shown in Fig. 5, two configurations of pressure-tapped plug were used. Static pressures were measured using a plug with two tappings abreast of each other and one inch apart. Surface pitot pressures were measured on a plug with three tappings, two of which were covered by pieces of razor blade. Each piece of razor blade, 0·25 inch square and originally 0·01

inch thick, had 0·004 inch ground from one face to reduce its thickness and produce a profile resembling that of a Stanton tube. It was cemented onto the plug, either directly or on top of one or two packing pieces of thin card, with its leading edge 0·001 inch aft of the upstream edge of the pressure tapping; the result was a family of pitots of varying heights and of approximate, but not strict, geometric similarity. Two plugs were used in the experiments, each carrying two pitots (the heights are given in Fig. 5). One plug, with pitots of height 0·0060 and 0·0127 inch, was fitted 1·25 inches to port of the centre line at stations 48·5, 38·5, 28·5 and 18·5 inches from the leading edge. The other was fitted on the centre line at distances of 54·5, 44·5, 34·5 and 24·5 inches from the leading edge and also, to provide a check between plugs, at 28·5 inches from the leading edge in the hole offset 1·25 inches to port.

3.3.4. *Transition indicator.* Transition regions were made visible by sublimation of azobenzene coatings from the surface of the plate. The coatings were sprayed on to the plate as a solution of one volume of the dry indicator in ten volumes of acetone. Quantities used, including wastage, were about 50 cc per square foot of plate surface. The distance between the spray gun and plate surface had to be controlled; when the gun was too close the plate received a very thin coating, initially a very wet 'wash', while if the gun was too far away the coating was thick and coarse-grained. It was necessary to run the tunnel for more than an hour (at a stagnation temperature of 40°C) to allow the transition pattern to develop fully. Later work on other models has shown that acenaphthene, which sublimes more rapidly, can be used successfully in this tunnel.

3.4. *Test Procedure.*

Tests were performed at a total temperature of 40°C and at total pressures of 25, 50, 100 and 200 inch *Hg* absolute. Resulting unit Reynolds numbers ranged from about $9{\cdot}4 \times 10^4$ to $7{\cdot}4 \times 10^5$ per inch. At each total pressure the skin friction was measured by the floating element, surface pitot and static pressures were recorded, and boundary-layer traverses were made. Since the readings of the skin-friction meter were not steady, about twenty readings were recorded during every pitot traverse. At each station and total pressure two traverses were made, one for pitot pressure and the other for temperature, and skin friction was thus obtained as the average of forty readings.

The instrumentation group is shown in Fig. 6. Its layout was chosen after preliminary tests to examine the possibility of interference between the various instruments in the group. The group was initially at its rearmost position on the plate and was subsequently moved forward.

Azobenzene sublimation patterns were obtained during separate runs.

4. *Results.*

The main results of the experiment are given in Tables 2 to 4, and the skin friction measurements and some features of the velocity profiles are illustrated in Figs. 10 to 16. Wall temperatures and freestream Mach numbers at the stations of the pitot traverses are shown in Fig. 7. The Mach numbers were determined from the ratio of freestream pitot pressure to tunnel total pressure. Transition positions are shown in Figs. 8 and 9.

4.1. *Accuracy.*

Traverse pitot pressures were measured to within $\pm 0{\cdot}02$ inch *Hg* and probe positions to within $\pm 0{\cdot}0005$ inch, but there will probably be a pitot displacement error on all readings. A special form of this error is noticeable close to the plate in the thickest boundary layers, for which the apparent velocity has a minimum away from the wall. It resembles errors noted[11] in traverses of laminar boundary layers in compressible flow. It seems likely that outside the immediate vicinity of the wall an outward displacement effect of approximately 0·15 pitot outside diameter should be expected. This is the value found[12] in low-speed flow, and there is some evidence[13] that compressibility does not affect displacement errors. Measurements at 25 inch and 50 inch *Hg* total pressure are probably subject to some viscous error on pitot readings. According to MacMillan[14], this error depends on a pitot Reynolds number based on the internal diameter of the probe; it becomes negligible only when the probe Reynolds number exceeds 200.

Velocities in the inner parts of the profiles at 25 inch *Hg* total pressure, where probe Reynolds numbers less than 20 occurred, might therefore be overestimated by several per cent. At 50 inch *Hg* total pressure the error should not exceed one per cent.

The recovery factors of the probes when used for measuring total temperature, determined from their readings outside the boundary layer, were rather low (0·9 approximately). The accuracy with which these factors applied within the boundary layer is not known, but the possibility of errors of several degrees C cannot be entirely discounted.

The static calibration of the skin-friction meter was repeatable to within ± 1 per cent of the maximum measurable force; i.e. approximately 0·5 gm. This latter corresponds to a C_f of slightly less than 0·002 at a total pressure of 200 inch *Hg*. This is only one factor in the overall accuracy of the meter. The meter was normally adjusted so that the element was recessed less than 0·0005 inch within its housing. Auxiliary tests showed that this procedure, which was adopted for convenience, was likely to reduce the force carried by the element by 3 per cent compared to the force it would bear if truly flush with the main surface. The area of the element and its surrounding gap was 6 per cent greater than the area of the element alone. Coles[4] has argued that the meter will record half the drag force on the gap, and has suggested that the effective shear stress on the gap will be of order twice that on the nearby smooth surface. Hence the combined error due to the gap and recessing the element may be an overestimation of shear stress by up to 3 per cent. Further sources of error in the instrument were zero shift and unsteadiness of reading which both occurred while the tunnel was running. These were examined, after the main measurements had been made, during some experiments by D. G. Mabey which formed part of a continuing investigation of techniques for skin-friction measurement. The zero shift was caused by bending of the plate and its supports under aerodynamic load and thermal stress. This bending tilted the meter and thus subjected the element to a gravitational force. For stations towards the rear of the plate the correction which has been applied to the meter reading is $-8{\cdot}5$ per cent (with an estimated uncertainty of ± 3–4 per cent) for the two highest total pressures. At other stations and total pressures the correction is larger and less certain. The unsteadiness of meter reading, much of which was due to an oscillating component in the tunnel flow at 6 *Hz* which coincided with the natural frequency of the element suspension, had an rms magnitude of about 5 per cent of the time-mean reading. Since the final values taken for skin friction were each the results of two tunnel runs, and were thus the average of some forty readings or more, meter unsteadiness is not expected to contribute significantly to the overall uncertainty of the measurements. The results presented in the tables have been corrected for zero shift, but no correction has been made for the combined effects of element recessing and gap force.

The overall accuracy of skin-friction coefficients derived from surface pitot measurements depends on the accuracy of the calibration function employed and on the accuracy of measurement of pitot height and pitot pressure. At best, that is for the largest pitot at 200 inch *Hg* total pressure, the accuracy in the present experiments was about ± 5 per cent. The calibration function used was the one presented by Hopkins and Keener in Fig. 18 of Ref. 15. It was extended to lower values of its constituent variables by relating results, from the present tests, of pitots having differing heights. This was possible because the pitot of $h = 0{\cdot}0127$ inch was always tested at stations between two at which the pitot of $h = 0{\cdot}0223$ inch was used. Consequently, if the reading of the larger pitot fell on the adopted calibration, the skin friction at the position of the smaller pitot could be deduced by interpolation and the reading of the smaller pitot then used to extend the calibration. Readings from the two small pitots were rejected, primarily because the readings of these pitots appeared to be unduly influenced by the presence of their larger neighbours.

4.2. *Transition Positions.*

Transition regions as indicated by azobenzene sublimation are shown in Fig. 8. Parts (a) and (b) of this figure show how, at a total pressure of 25 inch *Hg*, the surface pattern changes with time. Parts (e) and (f) show the same effect at a total pressure of 200 inch *Hg*. Although the later photographs illustrate the transition region more clearly, the actual position of transition can in each case be estimated quite well from the earlier photograph; i.e. the position of transition deduced from the photographs is not

critically dependent on the time allowed for the pattern to form.

The variation of transition Reynolds number with total pressure is given in Fig. 9. The loci of maximum and minimum surface pitot pressures are also shown. The surface pitots indicate a broader transition region than does the sublimation technique.

4.3. *Skin-friction Measurements.*

Skin friction measurements are listed in Table 2. It is found, by comparing skin-friction coefficients with rate of growth of momentum thickness, that there is an imbalance in the momentum equation indicative of flow convergence along the plate centre line. Further evidence of convergence is provided by the sublimation patterns, Figs. 8a, b and c, which show traces downstream from deliberate leaks through two pressure tappings. This convergence is very slight, and probably will not give rise to any perceptible spanwise variation of such parameters as boundary-layer thickness and profile shape parameter. Nevertheless, its contribution to the momentum equation is sufficiently large (in places, of order 25 per cent) to rule out the use of length of streamwise run as a meaningful scale for the boundary layer. For this reason, in presenting the skin friction measurements, Reynolds number based on momentum thickness is taken to be the only parameter with which they can profitably be correlated.

Fig. 10 shows skin-friction coefficient plotted as a function of momentum-thickness Reynolds number. The floating element and surface pitot measurements made at high Reynolds number (total pressures of 100 and 200 inch *Hg*) are in fairly close agreement with each other. At the lower Reynolds numbers, however, (i.e. total pressures of 25 and 50 inch *Hg*) there is some doubt about the reliability of the present skin-friction measurements. No floating-element results have been given, and those obtained with the surface razor blades appear rather low compared with the trend of the data at higher Reynolds numbers. The principal sources of uncertainty are the lower accuracy of pressure measurement at the lower tunnel pressures and the possibility of cumulative error in extending the razor-blade calibration (as described in Section 4.1) down to low Reynolds numbers. In Fig. 10 a mean line is drawn through the present data, opening into a fan to reflect the greater uncertainty of the measurements at low Reynolds number. This mean behaviour is compared in Fig. 11 with the correlation of Spalding and Chi and with data at $M \sim 4$ from other sources[16,17,18]. All data have been corrected to $M = 4$ using intermediate enthalpy theory. Most of the data for $R\delta_2 < 10000$ suggest that the present measurements in the lower part of this range did indeed err on the low side. At high $R\delta_2$ the present measurements are higher than the few available data from other sources, but are in good agreement with the correlations of Spalding and Chi (shown) and Winter and Gaudet (see Fig. 1).

4.4. *Velocity Profiles.*

Profiles from the experiments are given in Table 3 and displacement and momentum thicknesses in Table 4. The profiles of Mach number follow directly from pitot traverses. To convert them into velocity profiles, local temperatures or densities are required. The table gives densities and velocities determined using measured temperatures and also by assuming a parabolic temperature distribution

$$\frac{T}{T_e} = \frac{T_r}{T_e} + \left(\frac{T_r}{T_e} - 1\right)\left(\frac{u}{u_e}\right)^2 . \tag{27}$$

There is good agreement between the profiles for measured temperature and those for a parabolic distribution if the recovery factor (equation (15)) is 0·89. The difference resulting from a recovery factor of unity is shown for a few examples. The effect of the different temperature assumptions on the integral parameters is illustrated in Table 4b.

The comparisons between theory and experiment which follow, use velocity profiles based on measured temperatures. No comparison with the predictions of compressibility transformations is illustrated, since it merely confirms the findings of Baronti and Libby[19]. Velocity profiles at Mach 4, when transformed and then scaled to fit with a corresponding incompressible profile in the wall region, lie appreciably within the incompressible profile for all values of y outside the wall region.

Comparison with other theories is made, first, in terms of the velocity defect $(u_e - u)/u_{\tau w}$—where $u_{\tau w} = (\tau_w/\rho_w)^{\frac{1}{2}}$—expressed as a function of y/δ. Fig. 12 shows theoretical velocity-defect profiles at $M = 4$ drawn from three sources; the correlation of Winter and Gaudet[8], the correlation of Maise and McDonald[20], and the sample velocity profile calculated by Bradshaw and Ferriss[10] ($M = 4$, $R\delta_2 = 149\,000$). The correlation of Maise and McDonald comes from an extension of the mixing-length arguments used by van Driest to derive the skin-friction relation of Section 2.2.3. It results in a unique velocity-defect law written in terms of a generalised velocity u^* ($= \sqrt{2h_o}$ arc sin $[u/\sqrt{2h_o}]$ in flow with constant stagnation enthalpy h_o throughout the boundary layer). Fig. 12 shows the spread of the correlation in natural coordinates for the range $R\delta_2 = 5000$ (upper line) to $R\delta_2 = 150\,000$ (lower line). To make the vertical scales compatible for the three theories, the friction velocity $u_{\tau w}$ appearing in the ordinate of Fig. 12 is in each case based on the theoretical wall shear stress and on a wall density corresponding to adiabatic flow with recovery factor unity. As the figure shows, the differences between the three theories are small.

In Fig. 13 one of these relations, that of Winter and Gaudet, is compared with some of the present experimental results. In this Figure $u_{\tau w}$ is based on the actual density at an adiabatic wall, δ is taken as y at $u/u_e = 0{\cdot}99$, and for clarity only a few points from each profile are plotted. The spread of the experimental profiles is appreciably greater than that between the three theories of Fig. 12 and reveals a systematic variation of defect with Reynolds number. At the higher Reynolds numbers the agreement with the theoretical line is very satisfactory, velocities being predicted to better than 2 per cent over virtually the whole of the boundary layer. The trend of the data away from this line as Reynolds number decreases is shown consistently by all the measured profiles and illustrates a phenomenon shown previously by Coles[4] to occur in incompressible flows.

Having previously shown[21] that, in incompressible flow, wall shear stress could be derived from the relation

$$\frac{u_e}{u_\tau} = \frac{1}{\kappa} ln\left(\frac{\delta u_\tau}{\nu}\right) + C + \frac{2\pi}{\kappa}, \tag{28}$$

Coles produced evidence[4] that the 'wake component' π in this equation was constant for $R\delta_2 > 6000$ in constant-pressure flow. Below this Reynolds number π decreased to a value of zero for $R\delta_2 \sim 400$. By plotting u/u_e against log y for the present profiles, and fitting a straight line in the inner 'logarithmic' region, it was possible to determine π from the ratio of the 'overshoot' from the logarithmic line to the slope of this line. In Fig. 14 the values of π so obtained are compared with the correlation of results in incompressible flow given by Coles*. Apparently the behaviour found at low speeds is qualitatively reproduced at $M = 4$, but at Reynolds numbers roughly four times as high.

Bradshaw[22**] has recently suggested that the departure from 'fully developed' turbulent behaviour at low Reynolds numbers is linked with increasingly important viscous effects in the outer part of the boundary layer. Indeed, it is easily shown for incompressible flow that, if Clauser's eddy-viscosity hypothesis[23] is followed, the ratio of mean viscous to turbulent shear stress in the outer part of the layer is of order $40/R\delta_2$, so viscous stresses are not entirely negligible when $R\delta_2 \sim 400$. An equivalent argument gives the ratio as $40\,\nu/v_e R\delta_2^{(u)}$ in compressible flow, and if mean behaviour across the layer is typified by some 'bulk' viscosity $\bar{\nu}$, the scaling on $R\delta_2$ for flows with equivalent viscous contamination in the outer part of the boundary layer becomes $\bar{\nu}\,\delta_2/v_e\,\delta_2^{(u)}$. A value for this factor of 4 at a Mach number of 4 seems quite plausible. However, as Fig. 4 shows, the decay of the wake component at $M = 4$ is not well described by a simple scaling of Coles' incompressible correlation; it takes place over a thirteenfold increase in $R\delta_2$ at low speeds but only a fivefold increase at $M = 4$.

---

*The wake component π was determined from uncorrected versions of the present profiles. If a probe displacement correction of 0·15 d were made the average value of π obtained at high $R\delta_2$ would fall to $\sim 0{\cdot}55$.

**The following discussion of behaviour at low Reynolds numbers was contributed by Dr. J. E. Green.

An important consequence of the reducing wake component is that values of skin-friction coefficient at low Reynolds numbers may be expected to be appreciably higher than those predicted by the asymptotic skin-friction formulae which are valid at high Reynolds number. At a given $R\delta_2$ the complete disappearance of π from its asymptotic (high $R\delta_2$) value will give an increase of roughly 15 per cent in C_f. As a crude guide to how this behaviour might affect the predictions of those skin friction laws which do not take account of it, Fig. 15 is given. It is assumed that skin friction increases linearly with reduction in π such that

$$\frac{C_f}{C_{fA}} = 1+0{\cdot}15\left(1-\frac{\pi}{\pi_A}\right)$$

where suffix A refers to quantities in the asymptotic formula. The correlation of Coles and the present results are used to suggest contours of constant $\Delta C_f/C_f$ on a chart of $R\delta_2$ against M. Beyond the lower bound, to the left of the figure, it seems likely that the only turbulent boundary layers that occur are artificially tripped. Beyond the right hand boundary it is suggested that the flow is 'fully turbulent' in the sense that significant viscous effects are confined to that part of the layer close to the wall. Some corroboration for the construction of Fig. 15 is provided by values of π extracted from the data obtained by Adcock, Peterson and McRee[24] at $M = 6$. Moreover, the increase of C_f at low $R\delta_2$ predicted in this figure is in broad agreement with the divergence at low $R\delta_2$ shown in Fig. 11 between measured values of C_f (from Refs. 16, 17 and 18) and those given by an asymptotic formula. Nevertheless, the figure should be considered tentative and its purpose primarily a cautionary one. When applying a skin-friction relation to flows which fall within the range of this figure, or when making comparisons with experiments which fall within its range, it would seem advisable to consider the possibility of departures from 'fully turbulent' behaviour.

The inner parts of some profiles from Fig. 13 are compared in Fig. 16. The figure contains the profiles with low wake strength and also the profile with the highest available Reynolds number. The effects of outward displacement errors up to 0·002 inch and of uncertainties in skin friction at low Reynolds number are shown. The data for low Reynolds number are thus represented by small quadrilaterals within which their true value should lie. The experimental results collapse quite well to a single law of the wall.

The two lines drawn on the figure are the correlation of Winter and Gaudet and the version of the law of the wall proposed by Coles[25] for incompressible flow. It has been remarked by Bradshaw and Ferriss that other data from compressible flow, when normalised using fluid properties at the wall, fit reasonably well to the incompressible form of the law of the wall. The version of this law plotted in Fig. 16 is based on Coles' tabulation, falling away from the logarithmic line in the transitional region $y\,u_\tau/\nu < 40$. Although the present data fit the line well at $y\,u_\tau/\nu \sim 80$, the slope of their logarithmic region is clearly lower than that of the incompressible line and it appears that the transitional region is narrower—confined to $y\,u_\tau/\nu < 25$, say.

The relation of Winter and Gaudet, which may be written

$$\frac{u}{u_{\tau w}} = \frac{u_{\tau i}}{u_{\tau w}}\left[6{\cdot}05\log\frac{yu_{\tau w}}{\nu_w}+6{\cdot}05\log\frac{u_{\tau i}}{u_{\tau w}}\cdot\frac{\nu_w}{\nu_e}+4{\cdot}05\right]$$

where $(u_{\tau i})^2 = \dfrac{\tau_w}{\rho_e}\sqrt{\dfrac{T_{oe}}{T_e}}$, is seen to correlate the data rather better than the incompressible line. In particular, the lower slope and higher intercept of the logarithmic line are well predicted. By virtue of the scaling chosen for their correlation Winter and Gaudet have opted not to describe velocity profiles in the transitional and viscous layers between the logarithmic region and the wall, so their analysis has no bearing on departures from the logarithmic line at low yu_τ/ν.

5. *Conclusions.*

Skin-friction measurements at high Reynolds number are close to the predictions of Spalding and Chi and of Winter and Gaudet. At low Reynolds number the skin-friction coefficients are less certain. Other skin-friction measurements and the collapse of the present velocity-profile measurements support the higher of two tentative trend lines faired through the skin-friction measurements at low Reynolds number. The higher trend diverges from the predictions of the 'asymptotic' skin-friction formulae which are the most successful at high Reynolds numbers.

Velocity profiles near the wall, when normalised with respect to fluid properties at the wall, show a logarithmic line which has a lower slope and higher intercept than in incompressible flow. This behaviour is well predicted by the correlation of Winter and Gaudet. Velocity-defect profiles at high Reynolds number are in reasonably good agreement with a number of proposed correlations. As Reynolds number decreases the velocity defect is observed to decrease as a result of the progressive decay of the wake component π of the velocity profile. This decay, which might be associated with the increasing importance of viscous effects in the turbulent outer layer, is thought to be the reason why asymptotic skin-friction formulae appear to underestimate skin-friction at low Reynolds numbers. At $M = 4$ the decay sets in at values of momentum-thickness Reynolds number roughly four times as high as in incompressible flow.

6. *Acknowledgements.*

The original measurements, obtained in the winter of 1963/64, seemed difficult to reconcile with the boundary layer correlations which Winter and Gaudet were beginning to develop at that time, and which ultimately took the form outlined in Section 2.2.5. The resolution of this difficulty stems largely from D. G. Mabey's improved assessment of the accuracy of the skin friction meter measurements (Section 4.1) and J. E. Green's argument on low Reynolds number effects (Section 4.4).

These important contributions are most gratefully acknowledged.

LIST OF SYMBOLS

$\bar{A}\,\bar{B}$	Parameters in van Driest's mixing-length theory (equation (21))
c	Coles' friction parameter (equation (19))
C	Additive constant in logarithmic inner law (equation (28))
C_f	Local skin-friction coefficient (equations(1))
F_c, F_x, F_δ	Compressibility factors (equations (2))
h	Height of surface pitot
h_o	Stagnation enthalpy
K, L, n	Constants in simple incompressible law (equation (3))
N	Approximate invariant between different theories (equation (8))
M	Mach number
r	Recovery factor (equation (15))
R	Unit Reynolds number (equations (1))
T	Static temperature
T_o	Stagnation temperature
u	Velocity
u^*	Generalised velocity ($= \sqrt{2h_o}\,\arcsin\,[u/\sqrt{2h_o}]$) in mixing-length theory for adiabatic flow
u_τ	Friction velocity ($= \sqrt{\tau/\rho}$)
x	Distance along the wall measured from the virtual origin of the turbulent layer
y	Distance away from the wall
α, β	Parameters in van Driest's mixing-length theory (equation (21))
γ	Ratio of specific heats
δ	Boundary layer thickness
δ_1	Displacement thickness
δ_2	Momentum thickness
κ	Inverse of slope of logarithmic velocity profile (equation (28))
λ	Scaling factor or ordinate in compressibility transformation
μ	Absolute viscosity
ν	Kinematic viscosity ($= \mu/\rho$)
π	Wake component of velocity profile (equation (28))
ρ	Density
τ	Shear stress

ϕ	General functional form of skin-friction law
ω	Exponent in viscosity/temperature relation ($\mu \sim T^{\omega}$)
Subscripts	
e	Denotes conditions in the external stream
r	Denotes 'recovery' conditions, at an adiabatic wall
w	Denotes conditions at the wall
s	Denotes Coles' 'substructure' reference condition
i	Denotes the equivalent conditions in incompressible flow
Superscripts	
u	Denotes 'kinematic' integral parameters
–	Denotes either (a) quantities in a transformed plane or (b) 'bulk' quantities representing some average for the whole boundary layer
	Denotes properties evaluated at an intermediate temperature

LIST OF REFERENCES

No.	*Author(s)*	*Title, etc.*
1	E. R. G. Eckert	Survey on heat transfer at high speeds. WADC TR 54–70 (1954) (P 49878).
2	S. C. Sommer and Barbara J. Short	Free-flight measurements of turbulent-boundary-layer skin friction in the presence of severe aerodynamic heating at Mach numbers from 2·8 to 7·0. NACA TN 3391 (A.R.C. 17614) (1950).
3	D. A. Spence	Distributions of velocity, enthalpy and shear stress in the compressible turbulent boundary layer on a flat plate. J. Fluid Mech., 8, 368–387 (1960) A.R.C. 21642 also R.A.E. Report Aero 2631 (1959).
4	D. E. Coles	The turbulent boundary layer in a compressible fluid. Project Rand Rep. R–403–PR (A.R.C. 24497) (1962).
5	E. R. van Driest	The turbulent boundary layer with variable Prandtl number. 50 *years of boundary layer research.* (Ed. H. Görtler and W. Tollmien) Braunschweig, F. Vieweg, 257–271 (1955).
6	L. Prandtl	Zur turbulenten Stromung in Röhren und längs Platten. Ergebn. Aerodyn. Versuchsanst. Göttingen, 4, 18–29 (1932).
7	D. B. Spalding and S. W. Chi	The drag of a compressible turbulent boundary layer on a smooth flat plate with and without heat transfer. *J. Fluid. Mech.* 18, 1, 117–143 (1964).
8	K. G. Winter and L. Gaudet ..	Turbulent boundary layer studies at high Reynolds numbers at Mach numbers between 0·2 and 2·8. R.A.E./TR 70251 (1970).
9	K. G. Winter, K. G. Smith and L. Gaudet	Measurements of turbulent skin friction at high Reynolds numbers at Mach numbers of 0·2 and 2·2. AGARDograph 97, 1, 97–123 (1965).
10	P. Bradshaw and D. H. Ferriss	Calculation of boundary-layer development using the turbulent energy equation II: compressible flow on adiabatic walls. *Published in J. of Fluid Mechanics Vol.* 46, 1, pp. 83–110. (1971) A.R.C. 28541 (1966).
11	R. J. Monaghan	The use of pitot tubes in the measurement of laminar boundary layers in supersonic flow. A.R.C. R. & M. 3056 (1955).
12	F. A. MacMillan	Experiments on pitot tubes in shear flow. A.R.C. R. & M. 3028 (1956).
13	G. B. Marson and G. M. Lilley	The displacement effect of pitot tubes in narrow wakes. Coll. of Aero. Rep. 107 (1956).
14	F. A. MacMillan	Viscous effects of pitot tubes at low speeds. *J. Roy. Aero. Soc.*, 58, 570–572 (1954).
15	E. J. Hopkins and E. R. Keener	Study of surface pitots for measuring turbulent skin friction at supersonic Mach numbers—adiabatic wall. NASA TN D–3478 (A.R.C. 29008) (1966).

16	C. J. Stalmach	Experimental investigation of the surface impact probe method of measuring local skin friction at supersonic speeds. Univ. of Texas Rep. DRL–410, CF–2675 (1958).
17	D. E. Coles	Measurements in the boundary layer on a smooth flat plate in supersonic flow III. Caltech. JPL Rep. 20–71 (A.R.C. 17109) (1953).
18	F. W. Matting, D. R. Chapman, J. R. Nyholm and A. G. Thomas	Turbulent skin friction at high Mach numbers and Reynolds numbers in air and helium. NASA TR R–82 (1961).
19	P. O. Baronti and P. A. Libby	Velocity profiles in turbulent compressible boundary layers. *AIAA J.* 4, 193–201 (1966).
20	G. Maise and H. McDonald . .	Mixing length and kinematic eddy viscosity in a compressible boundary layer. *AIAA J.* 6, 73–80 (1968).
21	D. E. Coles	The law of the wake in the turbulent boundary layer. *J. Fluid Mech.* 1, 191–226 (1956).
22	P. Bradshaw	Special topics in turbulent flows. Contribution to VKI Lecture series. 10: "*Turbulent boundary layers.*" Von Karman Institute, Belgium, January 27–31, 1969.
23	F. H. Clauser	The turbulent boundary layer. *Advances in Applied Mechanics* IV 1–51 New York, Academic Press Inc. (1956).
24	J. B. Adcock, J. B. Peterson, Jr. and D. I. McRee	Experimental investigation of a turbulent boundary layer at $M = 6$, high Reynolds numbers, and zero heat transfer. NASA TN D–2907 (1965).
25	D. E. Coles	The law of the wall in turbulent shear flow. 50 *years of boundary layer research.* (Ed. H. Görtler and W. Tollmien) Braunschweig, F. Vieweg, 153–163 (1955).

TABLE 1

Compressibility Factors from Various Theories.
(for adiabatic flow at $M = 4$ and freestream total temperature 313°K)

Ref.	Author(s)	F_c	F_x	F_δ	$F_c F_\delta$	$F_c (F_\delta)^{\frac{1}{n-1}}$ ($n = 5$)	Notes
1	Eckert	3·05	0·114	0·349	1·07	2·34	
2	Sommer and Short	2·84	0·129	0·366	1·04	2·21	
4	Coles	2·09	—	0·524	1·09	1·78	$R\delta_2 \approx 1900$
		2·74	—	0·399	1·09	2·18	$R\delta_2 \approx 46000$
5	Van Driest	2·73	0·131	0·358	0·980	2·11	$\mu \sim T^{0·76}$
		2·73	0·105	0·286	0·782	2·00	$\mu \sim T^{0·93}$
		2·73	0·104	0·284	0·777	1·99	true viscosity
7	Spalding and Chi	2·65	0·147	0·396	1·05	2·10	
8	Winter and Gaudet	2·05	0·927	1·90	3·90	2·41	

TABLE 2

Local Skin-Friction Coefficients.

X in from l.e.	P_o in Hg	C_f Floating element	C_f Surface pitot $h = 0{\cdot}0223$	Interpolation from Table 3 $R\delta_2$	M_e
54·75	200		0·00100		
48·75					
44·75			0·00106	24035	3·934
44·5		0·00103		23820	3·934
38·75					
34·75			0·00106	18695	3·953
34·5		0·00108		18590	3·953
28·75			0·00105	16180	3·955
24·75			0·00112	14125	3·958
24·5		0·00115		13945	3·957
18·75					
14·75					
54·75	100		0·00115		
48·75					
44·75			0·00116	12455	3·926
44·5		0·00114		12360	3·926
38·75					
34·75			0·00120	9480	3·942
34·5		0·00124		9420	3·942
28·75			0·00123	8125	3·940
24·75			0·00139	7035	3·942
24·5		0·00137		6930	3·942
18·75					
14·75					
54·75	50		0·00123		
48·75					
44·75			0·00120	6504	3·915
38·75					
34·75			0·00124	5065	3·932
28·75			0·00132	3910	3·933
24·75			0·00152	3115	3·943
54·75	25		0·00174		
48·75					
44·75			0·00145	3455	3·897
38·75					

TABLE 3

Boundary Layer Profiles

Measurements at P_o = 25 in Hg			Derived ratios for different temperature distributions					
			Measured temp.		Quadratic, r = 0.89		Quadratic, r = 1.00	
y in	M	M/M_e	u/u_e	ρ/ρ_e	u/u_e	ρ/ρ_e	u/u_e	ρ/ρ_e
00006	08080	02069	03782	02993	03774	03005	03916	02792
00016	09339	02391	04296	03098	04288	03110	04441	02900
00056	17275	04424	06896	04116	06890	04122	07045	03943
00106	21735	05566	07880	04989	07906	04956	08032	04802
00156	24061	06162	08341	05458	08334	05467	08441	05328
00206	25655	06570	08596	05841	08592	05846	08687	05720
00256	27215	06969	08825	06237	08821	06242	08904	06127
00306	28760	07365	09028	06656	09027	06656	09097	06554
00406	32014	08198	09401	07604	09402	07604	09447	07531
00506	34610	08863	09651	08434	09652	08433	09679	08385
00606	36800	09424	09833	09185	09835	09182	09846	09157
00706	38041	09742	09926	09631	09928	09627	09934	09616
00806	38601	09885	09965	09839	09969	09833	09971	09828
00906	38893	09960	09983	09953	09989	09941	09990	09940
01006	39106	10014	09999	10031	10004	10021	10004	10021
01106	39026	09994	09991	10005	09998	09991	09998	09991

Measurements at P_o = 100 in Hg			Derived ratios for different temperature distributions					
			Measured temp.		Quadratic, r = 0.89		Quadratic, r = 1.00	
y in	M	M/M_e	u/u_e	ρ/ρ_e	u/u_e	ρ/ρ_e	u/u_e	ρ/ρ_e
00006	07851	01999	03676	02958	03673	02963	03812	02750
00016	13561	03453	05804	03540	05800	03544	05967	03349
00056	18055	04598	07079	04218	07078	04220	07229	04045
00106	20970	05340	07743	04756	07740	04760	07872	04602
00156	23203	05909	08172	05227	08171	05229	08286	05085
00206	25354	06456	08533	05724	08533	05726	08631	05596
00256	27443	06988	08840	06250	08840	06250	08921	06136
00306	29639	07548	09121	06847	09122	06846	09186	06750
00356	31563	08038	09325	07429	09340	07405	09390	07327
00406	33569	08548	09538	08032	09541	08026	09577	07966
00456	35535	09049	09704	08694	09717	08672	09740	08632
00506	37251	09486	09850	09274	09855	09266	09866	09244
00556	38309	09755	09927	09657	09933	09646	09938	09635
00606	38923	09912	09972	09879	09976	09871	09978	09867
00656	39195	09981	09993	09976	09995	09972	09995	09971
00706	39263	09998	09996	10005	10000	09998	10000	09997

Orders of most significant columns in tables

Quantity	Order
y	10
All others	1

a. Pilot run 42in from plate leading edge.

TABLE 3—*continued*

Measurements at P_o = 45 in Hg			Derived ratios for different temperature distributions					
			Measured temp.		Quadratic, r = 0.89		Quadratic, r = 1.00	
y in	M	M/M_e	u/u_e	ρ/ρ_e	u/u_e	ρ/ρ_e	u/u_e	ρ/ρ_e
00006	05940	01521	02849	02850	02844	02861	02958	02643
00016	10876	02785	04887	03248	04879	03259	05040	03053
00056	17971	04602	07058	04252	07068	04240	07219	04064
00106	20849	05339	07732	04768	07726	04775	07858	04616
00156	23152	05929	08179	05255	08174	05261	08289	05116
00206	24969	06394	08466	05704	08484	05680	08584	05548
00256	26917	06893	08781	06162	08779	06164	08864	06047
00306	28854	07389	09040	06681	09039	06682	09108	06581
00406	32127	08227	09415	07635	09413	07639	09458	07566
00506	35426	09072	09719	08712	09722	08707	09745	08667
00606	37533	09612	09888	09449	09891	09443	09900	09426
00706	38440	09844	09955	09777	09957	09773	09961	09766
00806	38619	09890	09967	09844	09970	09839	09972	09835
00906	38929	09969	09987	09964	09992	09955	09992	09953
01006	38885	09958	09986	09943	09989	09938	09990	09936
01106	38973	09980	09993	09975	09995	09971	09995	09970
01156	39017	09991	09996	09992	09998	09988	09998	09987

Measurements at P_o = 200 in Hg			Derived ratios for different temperature distributions					
			Measured temp.		Quadratic, r = 0.89		Quadratic, r = 1.00	
y in	M	M/M_e	u/u_e	ρ/ρ_e	u/u_e	ρ/ρ_e	u/u_e	ρ/ρ_e
00006	10789	02743	04839	03212	04837	03215	04999	03010
00006	10789	02743	04839	03212	04837	03215	04999	03010
00016	14975	03807	06237	03725	06236	03726	06400	03537
00026	16394	04167	06643	03935	06641	03937	06801	03754
00036	17422	04429	06916	04100	06914	04102	07069	03924
00046	18188	04623	07109	04229	07107	04231	07258	04057
00056	18981	04825	07299	04370	07298	04371	07444	04201
00066	19549	04969	07430	04473	07428	04475	07571	04308
00076	20118	05114	07559	04577	07555	04582	07693	04418
00086	20777	05281	07697	04708	07696	04710	07830	04550
00096	21131	05371	07772	04777	07769	04780	07900	04623
00106	21613	05494	07869	04874	07866	04878	07994	04723
00156	23867	06067	08287	05359	08284	05364	08394	05224
00206	25977	06603	08626	05860	08624	05862	08718	05737
00256	28166	07160	08932	06425	08933	06424	09009	06316
00306	30307	07704	09197	07017	09196	07017	09256	06927
00356	32527	08268	09436	07679	09435	07679	09479	07609
00406	34574	08789	09629	08331	09629	08330	09659	08280
00456	36552	09291	09796	08996	09796	08997	09812	08967
00456	36547	09290	09795	08996	09795	08995	09812	08965
00506	38081	09680	09910	09541	09912	09538	09919	09524
00556	38928	09895	09971	09848	09972	09847	09974	09843
00606	39260	09980	09995	09969	09995	09970	09995	09969
00656	39345	10001	10001	10001	10000	10002	10000	10002

Orders of most significant columns in tables

Quantity	Order
y	10
All others	1

a. Pilot run 42in from plate leading edge.

TABLE 3—*continued*

Measurements at P_o = 25 in Hg			Derived ratios for different temperature distributions					
			Measured temp.		Quadratic, r = 0.89		Quadratic, r = 1.00	
y in	M	M/M_e	u/u_e	ρ/ρ_e	u/u_e	ρ/ρ_e	u/u_e	ρ/ρ_e
00007	08251	02116	03839	03039	03847	03025	03991	02812
00009	08209	02105	03821	03035	03830	03022	03973	02809
00011	09386	02407	04300	03134	04309	03121	04462	02911
00013	09386	02407	04300	03134	04309	03121	04462	02911
00015	10144	02602	04595	03206	04605	03193	04763	02984
00017	10815	02774	04849	03272	04858	03260	05019	03054
00022	12529	03213	05460	03463	05469	03452	05635	03252
00027	14297	03667	06036	03690	06044	03680	06210	03487
00037	15978	04098	06532	03935	06541	03925	06702	03739
00047	16998	04360	06815	04093	06820	04086	06976	03905
00057	18307	04695	07159	04302	07154	04308	07303	04134
00067	18758	04811	07258	04394	07263	04388	07409	04217
00087	19737	05062	07483	04576	07488	04569	07628	04403
00107	21167	05429	07792	04854	07795	04850	07925	04693
00132	21940	05627	07946	05015	07950	05010	08074	04858
00157	22912	05876	08133	05221	08134	05220	08250	05074
00207	24454	06272	08404	05570	08403	05571	08507	05435
00257	26340	06756	08694	06038	08699	06031	08788	05909
00307	28038	07191	08940	06469	08937	06474	09013	06366
00357	29337	07524	09110	06822	09103	06832	09168	06735
00407	30639	07858	09262	07197	09256	07207	09312	07122
00457	32171	08251	09427	07660	09422	07669	09466	07598
00507	33752	08657	09583	08160	09577	08170	09610	08114
00607	35966	09224	09782	08893	09772	08911	09790	08878
00707	37666	09660	09915	09493	09905	09513	09913	09498
00807	38703	09927	09991	09871	09980	09893	09982	09890
00907	38998	10002	10013	09978	10001	10003	10000	10003

Measurements at P_o = 100 in Hg			Derived ratios for different temperature distributions					
			Measured temp.		Quadratic, r = 0.89		Quadratic, r = 1.00	
y in	M	M/M_e	u/u_e	ρ/ρ_e	u/u_e	ρ/ρ_e	u/u_e	ρ/ρ_e
00007	11782	03000	05173	03363	05199	03330	05364	03128
00009	12030	03064	05260	03391	05287	03358	05452	03157
00011	12858	03274	05543	03489	05570	03456	05736	03258
00013	13638	03473	05799	03587	05825	03554	05992	03359
00015	14204	03617	05978	03661	06004	03629	06170	03436
00017	14585	03714	06095	03714	06121	03681	06287	03490
00022	15416	03926	06343	03831	06369	03800	06532	03612
00027	16042	04085	06521	03924	06547	03893	06708	03709
00032	16509	04204	06651	03995	06676	03966	06835	03783
00037	16825	04284	06735	04047	06761	04016	06919	03835
00047	17589	04479	06935	04171	06960	04141	07114	03963
00057	18115	04613	07069	04259	07093	04230	07244	04055
00067	18733	04770	07218	04367	07243	04338	07390	04167
00087	19678	05011	07436	04541	07461	04511	07602	04345
00107	20667	05263	07653	04729	07676	04700	07811	04540
00132	21732	05534	07874	04939	07894	04915	08020	04761
00157	22760	05796	08071	05157	08090	05132	08209	04985
00182	23788	06058	08254	05386	08274	05360	08385	05219
00207	24727	06297	08414	05601	08432	05576	08535	05443
00257	26628	06781	08708	06063	08725	06040	08813	05921
00307	28499	07257	08967	06551	08980	06531	09053	06426
00357	30371	07734	09196	07073	09208	07054	09267	06965
00407	32203	08200	09398	07614	09407	07599	09452	07527
00457	34044	08669	09579	08191	09586	08179	09618	08124
00507	35742	09102	09728	08753	09734	08742	09756	08704
00557	37246	09485	09849	09274	09854	09264	09866	09242
00607	38334	09762	09932	09660	09935	09655	09940	09644
00657	38912	09909	09905	10008	09975	09867	09977	09863
00707	39132	09965	10004	09923	09991	09949	09991	09947
00757	39214	09986	09992	09988	09996	09979	09997	09979
00807	39263	09999	09997	10005	10000	09999	10000	09999

Orders of most significant columns in tables

Quantity	Order
y	10
All others	1

b. 46in from plate leading edge.

TABLE 3—*continued*

Measurements at P_o = 50 in Hg			Derived ratios for different temperature distributions					
			Measured temp.		Quadratic, r = 0.89		Quadratic, r = 1.00	
y in	M	M/M_e	u/u_e	ρ/ρ_e	u/u_e	ρ/ρ_e	u/u_e	ρ/ρ_e
00007	09767	02495	04439	03158	04454	03138	04610	02929
00009	10521	02687	04677	03301	04743	03211	04903	03004
00011	11373	02905	05041	03320	05057	03300	05221	03096
00013	12047	03077	05280	03396	05297	03375	05462	03174
00015	13021	03326	05613	03512	05629	03492	05795	03294
00017	13536	03457	05781	03576	05797	03557	05964	03361
00022	14894	03804	06203	03762	06220	03741	06384	03551
00027	15657	03999	06428	03871	06443	03853	06605	03666
00032	16267	04155	06599	03965	06615	03946	06775	03762
00037	16853	04305	06757	04058	06774	04038	06931	03857
00047	17541	04480	06938	04170	06954	04151	07108	03973
00057	18084	04619	07077	04261	07091	04244	07242	04069
00072	18896	04827	07275	04402	07287	04387	07433	04216
00087	19671	05025	07450	04549	07466	04530	07607	04363
00107	20656	05276	07671	04731	07680	04719	07814	04559
00132	21714	05546	07885	04948	07897	04933	08023	04779
00157	22743	05809	08084	05164	08093	05152	08212	05004
00257	26532	06777	08698	06071	08718	06043	08806	05923
00307	28275	07222	08955	06505	08959	06499	09033	06393
00357	30056	07677	09165	07016	09179	06995	09240	06904
00407	31667	08089	09354	07477	09359	07470	09407	07393
00457	33364	08522	09531	07994	09530	07997	09566	07936
00507	34988	08937	09679	08526	09678	08527	09704	08482
00607	37430	09561	09877	09369	09876	09371	09886	09352
00707	38687	09882	09971	09821	09968	09828	09971	09823
00807	39026	09968	09994	09948	09991	09954	09992	09952
00907	39147	09999	10004	09990	10000	09999	10000	09999

Measurements at P_o = 200 in Hg			Derived ratios for different temperature distributions					
			Measured temp.		Quadratic, r = 0.89		Quadratic, r = 1.00	
y in	M	M/M_e	u/u_e	ρ/ρ_e	u/u_e	ρ/ρ_e	u/u_e	ρ/ρ_e
00007	12691	03228	05462	03491	05512	03429	05678	03231
00009	13062	03322	05586	03536	05636	03475	05803	03278
00011	13729	03492	05803	03620	05852	03559	06019	03365
00013	14271	03630	05972	03693	06023	03632	06189	03439
00015	14766	03755	06125	03760	06174	03700	06339	03509
00017	15181	03861	06248	03819	06295	03759	06462	03570
00022	15980	04064	06479	03936	06527	03877	06689	03692
00027	16548	04208	06636	04022	06684	03964	06843	03782
00032	17025	04330	06764	04098	06812	04040	06969	03860
00037	17414	04429	06866	04161	06913	04104	07068	03926
00042	17816	04531	06967	04229	07016	04171	07169	03995
00047	18149	04616	07051	04285	07099	04228	07250	04053
00057	18772	04774	07204	04392	07249	04337	07397	04166
00077	19954	05075	07476	04608	07520	04554	07659	04390
00097	20859	05305	07672	04781	07714	04729	07847	04570
00117	21817	05549	07868	04973	07909	04923	08034	04770
00137	22538	05732	08006	05123	08046	05075	08167	04926
00157	23360	05941	08158	05303	08196	05254	08310	05111
00182	24335	06189	08329	05521	08365	05475	08471	05338
00207	25260	06424	08481	05737	08515	05692	08614	05562
00232	26241	06674	08633	05976	08665	05932	08756	05809
00257	27182	06913	08770	06214	08800	06170	08884	06055
00307	29073	07394	09025	06712	09050	06675	09119	06575
00357	30920	07864	09244	07237	09267	07201	09322	07116
00407	32557	08280	09422	07723	09440	07694	09483	07624
00457	32712	08319	09438	07770	09455	07742	09497	07674
00457	34517	08778	09612	08340	09625	08317	09655	08267
00507	36231	09214	09761	08911	09771	08894	09796	08859
00557	37637	09572	09872	09401	09880	09395	09899	09367
00557	37615	09566	09870	09395	09879	09376	09889	09359
00607	38519	09796	09937	09719	09944	09704	09949	09695
00657	38956	09907	09969	09876	09975	09865	09977	09861
00707	39158	09958	09985	09948	09989	09940	09990	09938

Orders of most significant columns in tables

Quantity	Order
y	10
All others	1

b. 46in from plate leading edge.

TABLE 3—*continued*

Measurements at P_o = 25 in Hg			Derived ratios for different temperature distributions					
			Measured temp.		Quadratic, r = 0.89		Quadratic, r = 1.00	
y in	M	M/M_e	u/u_e	ρ/ρ_e	u/u_e	ρ/ρ_e	u/u_e	ρ/ρ_e
00007	08927	02293	04139	03070	04127	03088	04276	02876
00009	09035	02321	04182	03080	04170	03097	04320	02886
00011	09000	02312	04167	03077	04156	03094	04306	02883
00013	10934	02809	04916	03264	04904	03280	05066	03074
00015	10893	02798	04902	03259	04888	03276	05051	03069
00017	11137	02861	04991	03285	04979	03302	05141	03096
00022	13149	03378	05692	03521	05676	03537	05846	03339
00027	14738	03786	06194	03736	06180	03750	06347	03558
00032	16934	04350	06816	04072	06806	04085	06962	03903
00037	18271	04693	07157	04300	07148	04311	07297	04137
00047	19312	04961	07404	04489	07395	04500	07538	04331
00057	19913	05116	07540	04604	07532	04614	07670	04449
00087	20786	05339	07728	04774	07716	04784	07852	04624
00107	21873	05619	07949	04997	07940	05008	08064	04854
00132	23038	05918	08167	05250	08160	05259	08275	05114
00157	24015	06169	08339	05472	08333	05481	08440	05342
00207	25752	06616	08621	05891	08615	05898	08709	05772
00257	27528	07071	08876	06347	08872	06352	08951	06241
00307	29135	07484	09084	06788	09082	06791	09148	06692
00357	30655	07875	09262	07229	09262	07228	09317	07143
00407	31993	08219	09409	07633	09409	07633	09453	07561
00457	33339	08564	09552	08039	09547	08055	09577	07995
00507	34702	08914	09666	08504	09665	08501	09694	08455
00607	36629	09409	09831	09160	09829	09163	09843	09137
00707	37947	09758	09927	09662	09933	09651	09938	09640
00807	38723	09948	09980	09937	09986	09924	09987	09922
00907	38941	10003	09996	10014	10001	10005	10001	10005
01007	39029	10025	10000	10050	10007	10037	10006	10038
01107	39102	10044	10007	10075	10012	10065	10011	10067
01157	38930	10000	09995	10010	10000	10000	10000	10000

Measurements at P_o = 100 in Hg			Derived ratios for different temperature distributions					
			Measured temp.		Quadratic, r = 0.89		Quadratic, r = 1.00	
y in	M	M/M_e	u/u_e	ρ/ρ_e	u/u_e	ρ/ρ_e	u/u_e	ρ/ρ_e
00007	11142	02839	04991	03235	04970	03263	05133	03059
00009	11658	02970	05166	03306	05156	03310	05320	03116
00011	12665	03227	05523	03413	05506	03435	05672	03236
00013	13465	03430	05783	03519	05770	03535	05937	03339
00015	14088	03589	05992	03589	05969	03616	06135	03423
00017	14532	03702	06128	03650	06106	03677	06272	03485
00022	15434	03932	06396	03780	06375	03805	06538	03618
00027	16055	04090	06574	03872	06551	03908	06712	03713
00032	16546	04216	06708	03950	06687	03974	06846	03792
00037	16947	04318	06815	04014	06794	04038	06951	03858
00047	17630	04492	06993	04126	06972	04151	07126	03973
00057	18275	04656	07154	04235	07133	04261	07283	04087
00067	18869	04807	07297	04340	07276	04365	07422	04195
00087	19940	05080	07539	04541	07520	04563	07660	04399
00107	20970	05343	07764	04735	07741	04764	07873	04605
00132	22049	05618	07975	04961	07957	04985	08081	04833
00157	23099	05885	08173	05185	08153	05210	08269	05065
00182	24126	06147	08351	05417	08333	05441	08441	05303
00207	25218	06425	08529	05674	08512	05697	08611	05567
00257	27270	06948	08833	06187	08817	06209	08900	06095
00257	27335	06964	08841	06206	08826	06225	08909	06112
00307	29373	07483	09106	06754	09091	06775	09157	06678
00357	31429	08007	09339	07352	09327	07371	09378	07291
00407	33464	08526	09543	07982	09533	07990	09569	07938
00457	35356	09008	09712	08603	09704	08618	09727	08576
00457	35380	09014	09715	08609	09705	08626	09729	08585
00507	37012	09430	09846	09173	09838	09188	09851	09164
00557	38273	09751	09937	09630	09933	09640	09937	09629
00607	38913	09914	09985	09859	09977	09875	09979	09871
00657	39161	09977	10000	09955	09994	09967	09994	09966
00707	39230	09995	10008	09974	09999	09993	09999	09992
00757	39261	10003	10007	09991	10001	10004	10001	10004
00807	39275	10006	10009	09995	10002	10009	10002	10010
00857	39254	10001	10007	09987	10000	10002	10000	10002

Orders of most significant columns in tables

Quantity	Order
y	10
All others	1

c. 42in from plate leading edge.

TABLE 3—*continued*

Measurements at P_o = 50 in Hg			Derived ratios for different temperature distributions					
			Measured temp.		Quadratic, r = 0.89		Quadratic, r = 1.00	
y in	M	M/M_e	u/u_e	ρ/ρ_e	u/u_e	ρ/ρ_e	u/u_e	ρ/ρ_e
00007	10048	02566	04573	03150	04563	03164	04720	02956
00009	09875	02522	04508	03131	04496	03148	04652	02939
00011	10919	02789	04904	03235	04891	03251	05053	03046
00013	11590	02960	05147	03308	05135	03324	05300	03121
00015	12653	03232	05518	03430	05505	03447	05672	03247
00017	12483	03144	05793	03534	05780	03550	05947	03354
00022	15636	03994	06447	03837	06437	03850	06600	03663
00027	16589	04237	06713	03984	06703	03996	06861	03814
00032	16569	04232	06708	03981	06699	03993	06856	03810
00037	17039	04352	06835	04055	06823	04068	06980	03888
00047	17895	04571	07054	04199	07044	04211	07196	04035
00057	18522	04731	07207	04309	07198	04320	07346	04147
00072	19397	04955	07413	04467	07403	04479	07546	04311
00097	20705	05135	07574	04597	07562	04612	07700	04448
00107	21164	05406	07795	04809	07786	04821	07916	04663
00132	22247	05683	08010	05033	08000	05045	08122	04895
00157	23320	05957	08204	05272	08190	05279	08312	05135
00207	25325	06469	08540	05737	08533	05744	08633	05615
00257	27149	06935	08810	06195	08806	06201	08889	06086
00307	29155	07447	09075	06734	09071	06741	09138	06642
00357	30921	07898	09280	07243	09278	07247	09332	07163
00407	32672	08345	09463	07777	09462	07779	09504	07711
00457	34406	08788	09628	08332	09627	08334	09656	08284
00507	35794	09143	09746	08799	09747	08799	09767	08763
00607	38052	09720	09920	09600	09922	09595	09929	09583
00707	38915	09940	09982	09916	09984	09912	09985	09910
00807	39115	09991	09994	09993	09998	09987	09998	09986
00907	39159	10002	10000	10005	10001	10003	10001	10004
01007	39203	10014	10003	10022	10004	10020	10003	10021
01107	39164	10004	09999	10009	10001	10005	10001	10006
01107	39169	10005	10000	10009	10001	10007	10001	10007

Measurements at P_o = 200 in Hg			Derived ratios for different temperature distributions					
			Measured temp.		Quadratic, r = 0.89		Quadratic, r = 1.00	
y in	M	M/M_e	u/u_e	ρ/ρ_e	u/u_e	ρ/ρ_e	u/u_e	ρ/ρ_e
00007	12538	03184	05413	03460	05458	03403		
00009	13503	03429	05731	03579	05777	03522		
00011	14190	03603	05948	03670	05995	03612		
00013	14706	03735	06105	03741	06154	03683		
00015	15108	03837	06223	03800	06274	03740		
00017	15453	03924	06321	03854	06374	03790		
00022	16196	04113	06533	03964	06585	03901		
00027	16711	04244	06680	04036	06725	03981		
00032	17194	04366	06797	04127	06853	04059		
00037	17617	04474	06895	04210	06962	04128		
00042	17910	04548	06983	04242	07036	04178		
00047	18318	04652	07085	04311	07137	04248		
00057	18973	04818	07244	04423	07294	04363		
00077	20133	05112	07506	04639	07556	04578		
00077	20127	05111	07504	04639	07555	04577		
00097	21119	05363	07717	04829	07765	04771		
00117	22049	05599	07901	05021	07950	04960		
00137	22909	05817	08062	05206	08111	05144		
00157	23717	06023	08208	05384	08256	05322		
00157	23793	06042	08218	05405	08269	05339		
00182	24805	06299	08393	05633	08439	05572		
00207	25876	06571	08567	05883	08607	05829		
00232	26940	06841	08734	06135	08763	06095		
00257	28169	07153	08912	06442	08931	06415		
00307	30105	07645	09168	06953	09170	06949		
00357	32199	08177	09415	07542	09400	07567		
00407	34279	08705	09635	08163	09600	08222		
00457	36244	09204	09809	08804	09768	08877		
00507	37905	09625	09940	09376	09896	09460		
00557	38816	09857	10003	09709	09961	09791		
00607	39231	09962	10034	09857	09990	09944		
00657	39361	09995	10041	09909	09999	09993		
00707	39361	09995	10037	09917	09999	09993		
00757	39366	09996	10032	09930	09999	09995		

Orders of most significant columns in tables

Quantity	Order
y	10
All others	1

c. 42in from plate leading edge.

TABLE 3—*continued*

Measurements at P_o = 25 in Hg			Derived ratios for different temperature distributions					
			Measured temp.		Quadratic, r = 0.89		Quadratic, r = 1.00	
y in	M	M/M_e	u/u_e	ρ/ρ_e	u/u_e	ρ/ρ_e	u/u_e	ρ/ρ_e
00007	10280	02625	04664	03169	04651	03186	04810	02978
00009	09415	02404	04327	03087	04315	03104	04469	02895
00011	09381	02395	04314	03084	04302	03101	04455	02892
00013	09381	02395	04314	03084	04302	03101	04455	02892
00015	10245	02616	04651	03164	04638	03182	04796	02975
00017	10498	02681	04746	03190	04734	03207	04894	03001
00022	12608	03220	05502	03424	05489	03440	05656	03240
00027	14346	03663	06065	03649	06052	03663	06218	03471
00037	16778	04284	06765	04011	06753	04025	06911	03843
00047	18435	04708	07187	04291	07176	04303	07325	04130
00057	19589	05002	07457	04500	07446	04513	07588	04346
00067	20243	05169	07602	04625	07591	04637	07728	04474
00087	21649	05528	07894	04905	07883	04918	08010	04764
00107	22664	05787	08087	05121	08078	05133	08197	04985
00107	23342	05961	08209	05273	08202	05282	08316	05138
00132	24318	06210	08375	05498	08371	05503	08477	05367
00157	25125	06416	08508	05688	08503	05694	08602	05563
00207	26539	06777	08723	06036	08718	06043	08806	05922
00257	28969	07398	09050	06682	09047	06686	09116	06586
00307	30353	07751	09214	07076	09213	07078	09271	06989
00367	32120	08202	09406	07605	09406	07605	09451	07532
00407	33653	08594	09555	08088	09557	08086	09591	08028
00457	35032	08946	09681	08540	09681	08538	09707	08494
00507	36485	09317	09800	09039	09802	09034	09818	09005
00607	38155	09743	09925	09637	09929	09629	09935	09618
00707	38874	09927	09977	09901	09980	09894	09982	09890
00807	39007	09961	09986	09950	09989	09943	09990	09941
00907	39016	09963	09987	09953	09990	09946	09991	09945
01007	39149	09997	09998	09997	09999	09996	09999	09996
01107	39070	09977	09993	09969	09994	09967	09994	09966
01157	39158	09999	09997	10005	10000	09999	10000	09999
01157	39158	09999	09997	10005	10000	09999	10000	09999
01157	39158	09999	09997	10005	10000	09999	10000	09999

Measurements at P_o = 100 in Hg			Derived ratios for different temperature distributions					
			Measured temp.		Quadratic, r = 0.89		Quadratic, r = 1.00	
y in	M	M/M_e	u/u_e	ρ/ρ_e	u/u_e	ρ/ρ_e	u/u_e	ρ/ρ_e
00007	10789	02735	04850	03179	04833	03202	04995	02998
00009	12026	03048	05296	03313	05278	03335	05444	03135
00011	13010	03298	05631	03430	05614	03452	05781	03255
00013	13848	03510	05902	03537	05885	03558	06052	03364
00015	14488	03672	06102	03622	06084	03643	06250	03452
00017	15001	03803	06175	03792	06239	03715	06404	03526
00022	15936	04040	06525	03832	06509	03851	06671	03667
00027	16566	04199	06699	03929	06683	03948	06843	03766
00032	17064	04326	06832	04009	06816	04027	06973	03848
00037	17538	04446	06955	04086	06939	04105	07094	03927
00047	18325	04645	07150	04221	07136	04238	07286	04065
00057	18951	04804	07300	04330	07285	04348	07432	04178
00067	19643	04979	07457	04458	07444	04474	07586	04308
00087	20840	05283	07713	04591	07703	04703	07837	04544
00107	21889	05549	07930	04396	07915	04914	08041	04762
00132	23272	05899	08185	05194	08173	05209	08289	05065
00157	24583	06231	08407	05495	08398	05506	08503	05370
00182	25736	06524	08590	05767	08581	05779	08677	05652
00207	26969	06836	08770	06076	08763	06086	08849	05968
00257	29348	07439	09083	06708	09076	06719	09143	06620
00257	29517	07482	09102	06757	09096	06766	09162	06669
00307	31836	08070	09361	07431	09357	07437	09406	07360
00357	34104	08645	09583	08137	09580	08143	09613	08088
00407	36234	09185	09763	08851	09763	08851	09782	08816
00407	36284	09197	09768	08867	09767	08868	09786	08834
00457	38010	09635	09897	09478	09899	09473	09907	09458
00507	38946	09872	09965	09815	09966	09813	09968	09808
00557	39317	09966	09989	09955	09991	09951	09992	09949
00607	39374	09981	09993	09976	09995	09972	09995	09971
00657	39426	09994	09993	10001	09998	09991	09999	09991
00707	39448	09999	09999	10001	10000	09999	10000	09999
00757	39477	10007	10001	10013	10002	10010	10002	10010
00807	39434	09996	09996	10001	09999	09994	09999	09994
00857	39442	09998	09998	10001	09999	09997	10000	09997

Orders of most significant columns in tables

Quantity	Order
y	10
All others	1

d. 36in from plate leading edge.

TABLE 3—*continued*

Measurements at P_o = 50 in Hg			Derived ratios for different temperature distributions					
			Measured temp.		Quadratic, r = 0.89		Quadratic, r = 1.00	
y in	M	M/M_e	u/u_e	ρ/ρ_e	u/u_e	ρ/ρ_e	u/u_e	ρ/ρ_e
00007	08646	02196	04016	02990	04000	03014	04148	02804
00009	09289	02359	04275	03045	04259	03069	04412	02860
00011	10400	02642	04707	03150	04690	03172	04850	02967
00013	11137	02829	04981	03225	04964	03249	05127	03044
00015	12334	03133	05406	03358	05388	03381	05554	03181
00017	13411	03406	05766	03491	05748	03512	05915	03316
00022	14971	03803	06248	03703	06233	03722	06398	03532
00027	16166	04106	06592	03879	06577	03898	06738	03714
00032	16809	04270	06768	03980	06752	03998	06910	03817
00037	17443	04431	06932	04085	06919	04101	07074	03923
00047	18369	04666	07164	04242	07150	04258	07300	04085
00057	19187	04874	07355	04390	07344	04404	07489	04233
00072	20082	05101	07560	04552	07545	04570	07684	04406
00087	21015	05338	07754	04739	07744	04752	07876	04593
00107	22052	05601	07959	04952	07951	04963	08075	04811
00132	23411	05946	08211	05244	08202	05256	08316	05113
00157	24615	06252	08413	05523	08408	05529	08512	05395
00207	27045	06870	08780	06122	08778	06124	08863	06007
00257	29234	07426	09067	06707	09067	06707	09135	06619
00307	31318	07955	09303	07311	09307	07305	09360	07224
00357	33359	08473	09510	07939	09515	07930	09553	07868
00407	35238	08950	09679	08551	09685	08540	09710	08496
00457	36861	09363	09809	09110	09818	09094	09833	09067
00507	38100	09677	09902	09552	09911	09534	09918	09520
00607	39146	09943	09974	09938	09985	09917	09986	09914
00707	39356	09996	09987	10018	09999	09995	09999	09995
00807	39361	09998	09989	10018	09999	09997	09999	09997
00907	39361	09998	09989	10018	09999	09997	09999	09997
01007	39361	09998	09989	10018	09999	09997	09999	09997

Measurements at P_o = 200 in Hg			Derived ratios for different temperature distributions					
			Measured temp.		Quadratic, r = 0.89		Quadratic, r = 1.00	
y in	M	M/M_e	u/u_e	ρ/ρ_e	u/u_e	ρ/ρ_e	u/u_e	ρ/ρ_e
00007	12919	03266	05589	03416	05579	03428	05747	03231
00009	13602	03439	05811	03503	05803	03513	05970	03318
00011	14363	03631	06050	03603	06042	03613	06208	03422
00013	14888	03764	06209	03676	06201	03685	06366	03496
00015	15334	03877	06340	03740	06333	03749	06497	03561
00017	15681	03965	06439	03791	06432	03799	06596	03613
00022	16436	04156	06650	03905	06643	03913	06804	03731
00027	16995	04297	06800	03994	06793	04001	06951	03821
00032	17458	04414	06921	04068	06914	04076	07069	03899
00037	17890	04523	07028	04142	07023	04148	07177	03973
00042	18274	04620	07125	04205	07118	04213	07269	04040
00047	18656	04717	07217	04273	07211	04280	07359	04108
00057	19348	04892	07379	04395	07372	04403	07517	04236
00077	20688	05231	07673	04648	07666	04656	07801	04496
00097	21804	05513	07898	04873	07893	04879	08020	04725
00117	22854	05779	08099	05091	08092	05099	08211	04955
00137	23900	06043	08282	05323	08278	05329	08389	05190
00157	24882	06291	08442	05553	08441	05555	08544	05421
00182	26039	06584	08624	05828	08621	05831	08715	05707
00207	27269	06895	08800	06139	08799	06140	08883	06025
00232	28573	07225	08974	06481	08973	06483	09047	06377
00257	29699	07509	09111	06793	09112	06791	09177	06695
00307	32231	08150	09389	07534	09392	07529	09439	07455
00307	32188	08139	09388	07516	09388	07516	09435	07442
00357	34502	08724	09605	08250	09609	08242	09640	08189
00407	36752	09293	09793	09004	09798	08996	09814	08966
00457	38462	09725	09918	09614	09925	09601	09931	09589
00507	39256	09926	09977	09898	09980	09891	09982	09888
00557	39488	09984	09991	09986	09996	09977	09996	09976
00607	39553	10001	09995	10011	10000	10001	10000	10001
00657	39554	10001	09994	10015	10000	10002	10000	10002
00707	39545	09999	09993	10011	10000	09998	10000	09998
00757	39540	09998	09994	10007	09999	09996	09999	09996
00807	39533	09996	09994	10003	09999	09994	09999	09994
00857	39524	09993	09992	10003	09998	09990	09998	09990
00907	39494	09986	09993	09986	09996	09979	09997	09979
00957	39502	09988	09992	09991	09997	09982	09997	09982
01007	39518	09992	09992	09999	09998	09988	09998	09988

Orders of most significant columns in tables

Quantity	Order
y	10
All others	1

d. 36in from plate leading edge.

TABLE 3—*continued*

Measurements at P_o = 25 in Hg			Derived ratios for different temperature distributions					
			Measured temp.		Quadratic, r = 0.89		Quadratic, r = 1.00	
y in	M	M/M_e	u/u_e	ρ/ρ_e	u/u_e	ρ/ρ_e	u/u_e	ρ/ρ_e
00007	08443	02158	03919	03031	03923	03025	04069	02813
00011	09226	02358	04237	03097	04241	03091	04393	02881
00015	11224	02868	05000	03291	05004	03286	05167	03082
00022	14772	03775	06179	03733	06184	03727	06349	03536
00037	19393	04956	07399	04486	07403	04481	07546	04313
00057	21672	05538	07846	04983	07889	04928	08016	04774
00097	24343	06221	08373	05520	08377	05516	08482	05379
00117	25330	06473	08516	05778	08537	05750	08634	05620
00137	26165	06687	08656	05963	08665	05955	08756	05832
00157	27228	06958	08816	06230	08818	06227	08901	06112
00207	29206	07464	09073	06767	09078	06760	09145	06661
00257	31064	07939	09290	07303	09295	07295	09348	07213
00307	32862	08398	09480	07847	09482	07844	09522	07778
00357	34429	08799	09627	08353	09630	08348	09659	08297
00407	35939	09184	09757	08861	09760	08855	09779	08821
00457	37215	09511	09859	09306	09861	09301	09873	09280
00507	38075	09730	09922	09618	09925	09611	09932	09599
00557	38578	09859	09958	09802	09962	09795	09965	09789
00607	38875	09935	09980	09909	09982	09905	09984	09902
00682	39137	10002	10015	09973	10000	10003	10000	10003
00757	39136	10001	10015	09973	10000	10002	10000	10002

Measurements at P_o = 100 in Hg			Derived ratios for different temperature distributions					
			Measured temp.		Quadratic, r = 0.89		Quadratic, r = 1.00	
y in	M	M/M_e	u/u_e	ρ/ρ_e	u/u_e	ρ/ρ_e	u/u_e	ρ/ρ_e
00007	11362	02887	05051	03266	05046	03273	05210	03070
00009	12098	03074	05312	03348	05307	03355	05473	03154
00011	13274	03373	05709	03490	05704	03496	05871	03300
00013	14127	03589	05981	03601	05977	03607	06143	03414
00015	14833	03769	06199	03696	06192	03704	06358	03514
00017	15385	03909	06362	03775	06356	03783	06519	03595
00022	16306	04143	06623	03913	06616	03921	06776	03737
00027	16969	04311	06801	04018	06795	04025	06953	03845
00032	17481	04441	06933	04103	06929	04109	07083	03931
00037	17935	04557	07048	04179	07044	04185	07196	04010
00047	18692	04749	07235	04309	07229	04316	07376	04145
00057	19484	04950	07418	04454	07413	04460	07556	04292
00067	20182	05127	07575	04582	07568	04591	07706	04428
00077	20811	05287	07707	04706	07702	04713	07835	04553
00087	21444	05448	07836	04835	07832	04840	07961	04684
00107	22609	05744	08063	05075	08057	05083	08177	04934
00132	23937	06081	08300	05368	08295	05375	08404	05236
00157	25361	06443	08533	05702	08528	05708	08627	05579
00182	26715	06787	08736	06036	08732	06042	08819	05923
00207	28163	07155	08931	06418	08931	06419	09007	06311
00232	29505	07496	09106	06777	09100	06785	09166	06688
00257	30880	07845	09266	07168	09260	07178	09315	07093
00282	32211	08184	09396	07585	09402	07576	09448	07503
00307	33417	08490	09527	07942	09521	07951	09559	07889
00332	34605	08792	09635	08327	09631	08334	09660	08284
00357	35676	09064	09729	08679	09723	08691	09745	08651
00382	36712	09327	09810	09039	09807	09046	09822	09017
00407	37568	09545	09876	09340	09872	09347	09883	09327
00432	38206	09707	09942	09633	09919	09576	09926	09563
00457	38654	09821	09955	09731	09951	09739	09955	09731
00482	38950	09896	09978	09836	09972	09848	09974	09843
00507	39111	09937	09989	09896	09983	09908	09984	09905
00532	39178	09954	09991	09925	09988	09932	09989	09930
00557	39256	09974	09999	09949	09993	09961	09994	09960
00607	39291	09982	10002	09961	09995	09974	09996	09973
00657	39358	10000	10007	09986	10000	09999	10000	09999

Orders of most significant columns in tables

Quantity	Order
y	10
All others	1

e. 32in from plate leading edge.

TABLE 3—*continued*

Measurements at P_o = 50 in Hg			Derived ratios for different temperature distributions					
			Measured temp.		Quadratic, r = 0.89		Quadratic, r = 1.00	
y in	M	M/M_e	u/u_e	ρ/ρ_e	u/u_e	ρ/ρ_e	u/u_e	ρ/ρ_e
00007	09130	02328	04203	03069	04200	03073	04351	02863
00009	09975	02544	04536	03145	04533	03150	04690	02942
00011	11303	02883	05032	03282	05030	03285	05193	03081
00013	12482	03183	05446	03414	05445	03418	05611	03219
00015	13504	03444	05788	03540	05784	03545	05951	03349
00017	14540	03708	06113	03679	06110	03683	06275	03492
00022	16151	04119	06585	03913	06580	03919	06740	03734
00027	17224	04393	06871	04087	06869	04089	07025	03910
00032	17895	04564	07043	04199	07041	04202	07193	04026
00037	18551	04731	07205	04312	07202	04316	07350	04143
00047	19379	04942	07401	04460	07396	04465	07539	04297
00057	20128	05133	07569	04599	07564	04606	07702	04443
00072	21179	05401	07756	04849	07786	04813	07916	04656
00097	22102	05637	07971	05000	07969	05003	08093	04852
00107	23263	05934	08190	05250	08186	05255	08300	05111
00132	24748	06312	08477	05544	08439	05594	08542	05460
00157	26046	06643	08645	05904	08642	05908	08735	05784
00207	28632	07302	09004	06577	09001	06582	09073	06478
00257	31008	07908	09283	07257	09284	07256	09337	07173
00307	33170	08460	09511	07911	09507	07917	09545	07854
00357	35151	08965	09690	08559	09688	08562	09713	08518
00407	36814	09389	09825	09132	09825	09132	09839	09106
00457	37961	09681	09912	09540	09912	09541	09919	09527
00507	38634	09853	09961	09784	09960	09787	09963	09780
00557	39001	09947	09986	09921	09986	09922	09987	09920
00607	39089	09969	09996	09946	09992	09955	09992	09953
00657	39139	09982	09997	09970	09995	09974	09996	09973
00707	39212	10001	10001	09999	10000	10001	10000	10001
00757	39219	10002	10001	10003	10001	10003	10001	10003
00807	39174	09991	10002	09978	09998	09987	09998	09986

Measurements at P_o = 200 in Hg			Derived ratios for different temperature distributions					
			Measured temp.		Quadratic, r = 0.89		Quadratic, r = 1.00	
y in	M	M/M_e	u/u_e	ρ/ρ_e	u/u_e	ρ/ρ_e	u/u_e	ρ/ρ_e
00007	12885	03262	05579	03419	05570	03430	05737	03233
00009	13649	03455	05828	03516	05820	03525	05987	03331
00011	14516	03675	06098	03632	06091	03640	06257	03450
00013	15065	03814	06263	03709	06256	03717	06421	03528
00015	15575	03943	06410	03784	06405	03791	06568	03604
00017	15984	04047	06529	03841	06521	03851	06683	03667
00022	16750	04241	06737	03962	06731	03970	06889	03789
00027	17308	04382	06883	04052	06877	04059	07034	03881
00032	17781	04502	07002	04133	06998	04137	07152	03962
00037	18205	04609	07109	04204	07104	04209	07255	04036
00042	18637	04718	07213	04278	07208	04284	07357	04113
00047	19027	04817	07305	04348	07301	04353	07447	04184
00057	19774	05006	07474	04486	07471	04490	07612	04325
00077	21104	05343	07705	04808	07755	04746	07887	04589
00097	22263	05636	07984	04984	07984	04983	08108	04833
00117	23431	05932	08197	05237	08199	05235	08313	05092
00137	24585	06224	08392	05500	08396	05496	08501	05361
00157	25687	06503	08566	05763	08571	05757	08667	05629
00182	27067	06852	08770	06105	08774	06100	08859	05983
00207	28440	07200	08951	06471	08959	06459	09033	06353
00207	28442	07201	08951	06471	08959	06460	09034	06353
00232	29748	07531	09116	06825	09121	06818	09186	06722
00257	31319	07929	09289	07286	09299	07270	09352	07188
00282	32614	08257	09422	07680	09434	07660	09478	07590
00307	33939	08592	09492	08193	09561	08076	09596	08018
00332	35288	08934	09670	08536	09681	08516	09706	08471
00357	36445	09227	09763	08932	09776	08907	09795	08874
00382	37460	09484	09839	09290	09855	09260	09867	09238
00407	38246	09682	09895	09575	09913	09540	09920	09527
00432	38800	09823	09936	09772	09952	09742	09956	09734
00457	39128	09906	09960	09892	09975	09862	09977	09858
00482	39285	09945	09971	09949	09985	09920	09987	09918
00507	39384	09971	09978	09986	09992	09957	09993	09956
00532	39423	09981	09980	10001	09995	09971	09995	09971
00557	39443	09986	09980	10011	09996	09979	09996	09978
00607	39503	10001	09986	10030	10000	10001	10000	10001

Orders of most significant columns in tables

Quantity	Order
y	10
All others.	1

e. 32in from plate leading edge.

TABLE 3—*continued*

Measurements at P_o = 50 in Hg			Derived ratios for different temperature distributions					
			Measured temp.		Quadratic, r = 0.89		Quadratic, r = 1.00	
y in	M	M/M_e	u/u_e	ρ/ρ_e	u/u_e	ρ/ρ_e	u/u_e	ρ/ρ_e
00007	10630	02695	04736	03238	04774	03187		
00009	11294	02864	04972	03317	05019	03256		
00011	12799	03245	05495	03488	05543	03427		
00013	14460	03666	06585	03100	06076	03641		
00015	15673	03974	06386	03872	06435	03813		
00017	16795	04258	06696	04045	06745	03986		
00022	18443	04676	07116	04318	07165	04260		
00027	19610	04972	07388	04530	07437	04470		
00032	20422	05178	07564	04686	07615	04623		
00037	21053	05338	07693	04815	07748	04747		
00047	21967	05570	07878	04999	07931	04933		
00057	22847	05793	08047	05182	08097	05119		
00072	24114	06114	08271	05464	08320	05400		
00087	25252	06403	08449	05743	08507	05665		
00107	26648	06757	08657	06091	08717	06007		
00132	28434	07210	08901	06561	08962	06472		
00157	30140	07642	09112	07033	09171	06944		
00207	33333	08452	09450	07999	09508	07901		
00257	36070	09146	09694	08900	09750	08798		
00307	37636	09593	09829	09526	09887	09414		
00357	38879	09858	09904	09906	09962	09792		
00407	39346	09976	09931	10091	09994	09965		
00457	39469	10007	09931	10154	10002	10011		

Measurements at P_o = 200 in Hg			Derived ratios for different temperature distributions					
			Measured temp.		Quadratic, r = 0.89		Quadratic, r = 1.00	
y in	M	M/M_e	u/u_e	ρ/ρ_e	u/u_e	ρ/ρ_e	u/u_e	ρ/ρ_e
00007	13112	03312	05589	03511	05642	03446	05589	03511
00009	14150	03574	05917	03648	05974	03579	05917	03648
00011	14841	03749	06125	03745	06185	03673	06125	03745
00013	15343	03876	06269	03821	06334	03744	06269	03821
00015	15832	03999	06409	03893	06474	03816	06409	03893
00017	16256	04106	06531	03953	06592	03880	06531	03953
00022	17038	04304	06745	04071	06803	04002	06745	04071
00027	17641	04456	06901	04169	06959	04100	06901	04169
00032	18142	04582	07030	04249	07084	04184	07030	04249
00037	18659	04713	07155	04338	07209	04274	07155	04338
00042	19088	04821	07260	04411	07310	04350	07260	04411
00047	19514	04929	07359	04486	07408	04427	07359	04486
00047	19554	04939	07369	04493	07417	04434	07369	04493
00057	20340	05138	07542	04640	07590	04582	07542	04640
00077	21830	05514	07844	04942	07896	04877	07844	04942
00097	23210	05863	08104	05233	08155	05169	08104	05233
00117	24601	06214	08345	05545	08393	05481	08345	05545
00137	25993	06565	08570	05869	08612	05812	08570	05869
00157	27284	06892	08761	06188	08799	06135	08761	06188
00182	28938	07309	08993	06607	09017	06572	08993	06607
00207	30700	07754	09209	07090	09226	07065	09209	07090
00207	30744	07766	09213	07105	09230	07078	09213	07105
00232	32369	08176	09392	07579	09404	07560	09392	07579
00257	34013	08591	09556	08082	09562	08072	09556	08082
00282	35561	08982	09688	08596	09698	08578	09688	08596
00307	36987	09342	09801	09087	09813	09064	09801	09087
00322	38114	09627	09886	09483	09897	09461	09886	09483
00357	38821	09806	09937	09738	09948	09717	09937	09738
00382	39246	09913	09968	09890	09977	09873	09968	09890
00407	39415	09956	09985	09942	09988	09935	09985	09942
00432	39508	09979	09990	09979	09995	09970	09990	09979
00457	39524	09983	09992	09983	09996	09975	09992	09983
00482	39546	09989	09987	10004	09997	09984	09987	10004
00507	39576	09996	09984	10025	09999	09995	09984	10025
00532	39575	09996	09980	10033	09999	09994	09980	10033
00557	39548	09989	09977	10025	09997	09984	09977	10025
00657	39607	10004	09988	10033	10001	10006	09983	10033
00757	39623	10008	09967	10082	10002	10012	09967	10082

Orders of most significant columns in tables

Quantity	Order
y	10
All others	1

f. 26in from plate leading edge.

TABLE 3—*continued*

Measurements at P_o = 100 in Hg			Derived ratios for different temperature distributions					
			Measured temp.		Quadratic, r = 0.89		Quadratic, r = 1.00	
y in	M	M/M_e	u/u_e	ρ/ρ_e	u/u_e	ρ/ρ_e	u/u_e	ρ/ρ_e
00007	12072	03061	05239	03413	05295	03342		
00009	13408	03399	05685	03576	05744	03502		
00011	14549	03689	06039	03731	06103	03653		
00013	15313	03883	06265	03840	06331	03761		
00015	15961	04047	06452	03935	06517	03857		
00017	16552	04197	06613	04028	06680	03947		
00022	17467	04429	06854	04176	06921	04094		
00027	18074	04583	07003	04282	07074	04196		
00032	18577	04710	07131	04363	07197	04283		
00037	19138	04853	07265	04462	07329	04383		
00047	19956	05060	07451	04611	07514	04534		
00057	20824	05280	07641	04775	07700	04701		
00067	21726	05509	07829	04950	07883	04883		
00077	22472	05698	07977	05101	08027	05038		
00087	23262	05898	08125	05269	08172	05209		
00107	24709	06265	08374	05598	08420	05537		
00132	26516	06723	08659	06029	08698	05974		
00157	28198	07150	08892	06465	08931	06409		
00182	29855	07570	09100	06920	09137	06863		
00207	31558	08002	09283	07431	09329	07357		
00232	33053	08381	09444	07875	09481	07813		
00257	34586	08769	09581	08377	09624	08303		
00282	35959	09117	09702	08832	09741	08760		
00307	37158	09421	09795	09251	09836	09175		
00332	38084	09656	09864	09583	09905	09503		
00357	38656	09801	09904	09794	09946	09711		
00382	39008	09890	09927	09926	09971	09840		
00407	39194	09938	09940	09995	09983	09909		
00432	39296	09963	09945	10038	09990	09946		
00457	39329	09972	09947	10050	09993	09959		
00482	39392	09988	09949	10079	09997	09982		
00507	39406	09991	09950	10083	09998	09987		
00532	39428	09997	09950	10095	09999	09995		

Orders of most significant columns in tables

Quantity	Order
y	10
All others	1

f. 26in from plate leading edge.

TABLE 3—*continued*

Measurements at P_o = 50 in Hg			Derived ratios for different temperature distributions					
			Measured temp.		Quadratic, r = 0.89		Quadratic, r = 1.00	
y in	M	M/M_e	u/u_e	ρ/ρ_e	u/u_e	ρ/ρ_e	u/u_e	ρ/ρ_e
00007	11667	02960	05135	03322	05153	03299		
00009	12329	03128	05367	03396	05385	03374		
00011	14002	03552	05917	03603	05935	03582		
00013	15562	03948	06386	03822	06404	03800		
00015	16663	04227	06694	03988	06711	03968		
00017	17807	04517	06991	04175	07009	04154		
00022	19581	04967	07415	04488	07432	04468		
00027	20595	05225	07639	04678	07653	04660		
00032	21351	05416	07796	04826	07810	04810		
00037	21916	05560	07906	04945	07922	04925		
00047	22891	05807	08092	05150	08106	05132		
00057	23854	06051	08266	05359	08277	05345		
00067	25251	06406	08495	05686	08508	05669		
00087	26456	06711	08678	05981	08691	05963		
00107	28157	07143	08918	06415	08927	06403		
00132	30288	07683	09181	07004	09189	06991		
00157	32320	08199	09402	07605	09409	07593		
00182	34150	08663	09582	08175	09586	08168		
00207	35706	09058	09696	08728	09721	08681		
00232	36759	09325	09801	09052	09807	09042		
00257	37723	09570	09877	09387	09880	09381		
00307	38740	09827	09952	09751	09953	09749		
00357	39250	09957	09988	09938	09989	09937		
00407	39393	09993	09998	09991	09998	09990		
00507	39508	10022	10004	10036	10006	10033		
00607	39554	10034	10007	10053	10009	10050		
00707	39548	10033	10006	10053	10009	10048		
00807	39508	10022	10004	10036	10006	10033		
00907	39427	10002	09997	10008	10000	10002		
01007	39410	09997	09998	09999	09999	09996		
01107	39422	10001	09999	10003	10000	10001		

Measurements at P_o = 200 in Hg			Derived ratios for different temperature distributions					
			Measured temp.		Quadratic, r = 0.89		Quadratic, r = 1.00	
y in	M	M/M_e	u/u_e	ρ/ρ_e	u/u_e	ρ/ρ_e	u/u_e	ρ/ρ_e
00007	13602	03439	05795	03522	05803	03513		
00009	14571	03684	06096	03653	06106	03641		
00011	15212	03846	06263	03771	06297	03731		
00013	16005	04047	06513	03860	06524	03847		
00015	16521	04177	06654	03941	06667	03926		
00017	16955	04287	06772	04008	06783	03995		
00022	17767	04492	06981	04141	06993	04127		
00027	18390	04650	07136	04246	07147	04233		
00032	18892	04777	07255	04334	07266	04321		
00037	19383	04901	07370	04422	07380	04410		
00042	19873	05025	07480	04513	07490	04500		
00047	20400	05158	07595	04612	07605	04600		
00057	21359	05401	07792	04803	07804	04788		
00077	23155	05855	08137	05177	08147	05164		
00087	23963	06059	08279	05355	08289	05344		
00097	24808	06273	08420	05550	08429	05537		
00107	25620	06478	08546	05745	08558	05730		
00117	26420	06680	08664	05938	08678	05926		
00137	28061	07095	08898	06358	08906	06346		
00137	28189	07128	08914	06393	08923	06380		
00157	29677	07504	09103	06795	09109	06785		
00182	31652	08003	09323	07369	09332	07355		
00207	33698	08520	09490	08060	09536	07984		
00232	35582	08997	09697	08607	09703	08598		
00257	37056	09369	09816	09112	09821	09101		
00282	38250	09671	09904	09536	09910	09524		
00307	38892	09834	09949	09769	09955	09757		
00332	39219	09916	09972	09889	09978	09877		
00357	39366	09953	09983	09942	09988	09932		
00382	39408	09964	09989	09949	09990	09947		
00407	39431	09970	09987	09966	09992	09956		
00457	39481	09983	09992	09982	09995	09974		
00507	39539	09997	09994	10007	09999	09996		
00607	39552	10000	09993	10015	10000	10001		
00707	39546	09999	09993	10011	10000	09999		

Orders of most significant columns in tables

Quantity	Order
y	10
All others	1

g. 22in from plate leading edge.

TABLE 3—*continued*

Measurements at P_0 = 100 in Hg			Derived ratios for different temperature distributions					
			Measured temp.		Quadratic, r = 0.89		Quadratic, r = 1.00	
y in	M	M/M_e	u/u_e	ρ/ρ_e	u/u_e	ρ/ρ_e	u/u_e	ρ/ρ_e
00007	13006	03301	05602	03473	05614	03457		
00009	13071	03317	05625	03479	05635	03465		
00011	14249	03616	06001	03632	06013	03618		
00013	15282	03879	06313	03775	06324	03762		
00015	16218	04116	06580	03914	06590	03901		
00017	16940	04299	06774	04028	06786	04015		
00022	18041	04579	07056	04211	07068	04197		
00027	18812	04775	07243	04345	07255	04331		
00032	19386	04920	07377	04449	07388	04435		
00037	19949	05063	07504	04552	07515	04540		
00047	21018	05334	07735	04757	07743	04747		
00057	21981	05579	07927	04954	07935	04943		
00067	22927	05819	08108	05151	08114	05144		
00077	23854	06054	08270	05359	08278	05349		
00087	24750	06282	08419	05567	08428	05555		
00107	26423	06706	08679	05970	08687	05960		
00132	28409	07210	08953	06487	08961	06475		
00157	30295	07689	09187	07005	09191	06998		
00232	35522	09016	09707	08627	09707	08626		
00257	36738	09324	09805	09043	09806	09041		
00282	37780	09589	09886	09408	09886	09408		
00307	38440	09756	09931	09651	09933	09646		
00357	39069	09916	09977	09877	09977	09877		
00407	39252	09963	09992	09942	09990	09945		
00457	39290	09972	09993	09959	09993	09959		
00507	39322	09980	09993	09974	09995	09971		
00607	39378	09995	09999	09991	09999	09992		
00707	39381	09995	10000	09991	09999	09993		
00807	39392	09998	10000	09995	09999	09997		

Orders of most significant columns in tables

Quantity	Order
y	10
All others	1

g. 22in from plate leading edge.

Measurements at P_o = 100 in Hg			Derived ratios for different temperature distributions					
			Measured temp.		Quadratic, r = 0.89		Quadratic, r = 1.00	
y in	M	M/M_e	u/u_e	ρ/ρ_e	u/u_e	ρ/ρ_e	u/u_e	ρ/ρ_e
00007	13861	03486	05850	03552	05877	03519		
00009	14967	03764	06187	03702	06216	03668		
00011	16142	04060	06526	03870	06553	03838		
00013	17096	04300	06784	04017	06811	03986		
00015	17879	04497	06978	04153	07011	04114		
00017	18553	04666	07150	04259	07176	04228		
00022	19754	04968	07430	04472	07454	04443		
00027	20561	05171	07607	04621	07629	04595		
00032	21171	05325	07731	04743	07756	04714		
00037	21867	05500	07874	04879	07894	04854		
00047	23210	05837	08125	05162	08145	05136		
00057	24562	06178	08357	05465	08377	05438		
00067	26068	06556	08596	05818	08614	05793		
00077	27621	06947	08816	06210	08835	06183		
00087	29252	07357	09032	06635	09045	06615		
00107	32385	08145	09383	07535	09395	07517		
00132	35354	08892	09664	08466	09670	08455		
00157	37366	09398	09826	09149	09831	09138		
00182	38582	09704	09916	09576	09920	09569		
00207	39289	09882	09965	09834	09969	09826		
00207	39289	09882	09965	09834	09969	09826		
00232	39576	09954	09986	09935	09988	09932		
00257	39720	09990	09997	09985	09997	09985		
00282	39786	10007	09999	10014	10002	10010		
00307	39823	10016	10003	10026	10004	10024		
00357	39849	10022	10003	10040	10006	10033		
00407	39872	10028	10004	10048	10007	10042		
00457	39852	10023	10003	10040	10006	10034		
00507	39849	10022	10003	10040	10006	10033		
00607	39849	10022	10003	10040	10006	10033		
00707	39783	10006	10001	10010	10002	10009		
00807	39749	09997	09979	10036	09999	09996		

Orders of most significant columns in tables

Quantity	Order
y	10
All others	1

h. 16in from plate leading edge.

Measurements at P_o = 200 in Hg			Derived ratios for different temperature distributions					
			Measured temp.		Quadratic, r = 0.89		Quadratic, r = 1.00	
y in	M	M/M_e	u/u_e	ρ/ρ_e	u/u_e	ρ/ρ_e	u/u_e	ρ/ρ_e
00007	14184	03571	05943	03611	05980	03566		
00009	15017	03781	06196	03724	06232	03680		
00011	15831	03986	06431	03841	06468	03797		
00013	16453	04142	06603	03936	06641	03891		
00015	17034	04289	06760	04024	06796	03982		
00017	17549	04418	06894	04108	06930	04065		
00022	18476	04652	07125	04262	07159	04221		
00027	19149	04821	07285	04379	07318	04340		
00032	19734	04968	07419	04485	07451	04446		
00037	20274	05104	07537	04586	07570	04547		
00042	20863	05252	07684	04673	07694	04660		
00047	21440	05398	07783	04810	07812	04774		
00057	22618	05694	08012	05051	08039	05017		
00072	24869	06261	08404	05550	08430	05517		
00087	25975	06540	08388	06078	08602	05780		
00097	27110	06825	08747	06089	08767	06061		
00107	28274	07118	08906	06389	08924	06362		
00117	29372	07395	09045	06684	09062	06658		
00137	31391	07903	09281	07251	09293	07232		
00137	31407	07907	09280	07260	09295	07236		
00157	33397	08408	09484	07859	09497	07839		
00182	35835	09022	09706	08641	09713	08628		
00207	37813	09520	09863	09316	09867	09309		
00232	38965	09810	09947	09725	09949	09722		
00257	39365	09911	09976	09869	09976	09869		
00282	39545	09956	09989	09934	09988	09935		
00307	39588	09967	09992	09950	09991	09951		
00332	39637	09979	09996	09967	09995	09969		
00357	39677	09989	09998	09983	09997	09984		
00382	39669	09987	09998	09979	09997	09981		
00407	39644	09981	09991	09979	09995	09972		
00457	39692	09993	09999	09988	09998	09989		
00507	39725	10001	10001	10000	10000	10002		
00607	39703	09996	09996	10000	09999	09994		
00707	39709	09997	09997	10000	09999	09996		

Orders of most significant columns in tables

Quantity	Order
y	10
All others	1

h. 16in from plate leading edge.

TABLE 4

Displacement and Momentum Thicknesses.

(a) *Integrals based on measured temperatures.*

X in from l.e.	M_e	$\frac{T_w}{T_{oe}}$	$10^{-5}\,R$/in	δ_1 in	δ_2 in	$R\delta_2$
*42	3·905	—	0·950	0·2626	0·0353	3349
	3·905	—	1·708	0·2573	0·0347	5931
	3·927	—	3·747	0·2305	0·0309	11574
	3·934	—	7·456	0·2150	0·0289	21530
46	3·899	0·917	0·939	0·2805	0·0375	3518
	3·915	0·919	1·869	0·2614	0·0355	6635
	3·927	0·908	3·763	0·2498	0·0346	12905
	3·932	0·888	7·474	0·2400	0·0336	25130
42	3·893	0·922	0·956	0·2535	0·0347	3318
	3·915	0·919	1·887	0·2441	0·0329	6214
	3·925	0·932	3·754	0·2330	0·0305	11458
	3·938	0·902	7·456	0·2203	0·0286	21630
36	3·916	0·928	0·951	0·2268	0·0306	2913
	3·937	0·933	1·880	0·2074	0·0283	5313
	3·945	0·932	3·723	0·1980	0·0263	9783
	3·955	0·929	7·400	0·1921	0·0260	19222
32	3·913	0·924	0·945	0·1798	0·0244	2304
	3·921	0·923	1·889	0·1795	0·0240	4520
	3·936	0·932	3·731	0·1789	0·0236	8811
	3·950	0·931	7·410	0·1715	0·0237	17532
26	3·943	0·921	1·862	0·1189	0·0182	3386
	3·933	0·918	3·718	0·1362	0·0203	7549
	3·959	0·916	7·381	0·1435	0·0204	15039
22	3·942	—	1·861	0·0994	0·0136	2523
	3·940	0·919	3·724	0·1179	0·0159	5904
	3·955	0·909	7·399	0·1196	0·0164	12125
16	3·976	—	3·661	0·0704	0·0095	3484
	3·972	0·924	7·338	0·0935	0·0127	9340

*Data from pilot run; wall temperature not measured.

TABLE 4 (Contd)

(b) *Illustration of the dependence of displacement and momentum thicknesses on the assumed temperature distribution.*

M_e	Temperature distribution	δ_1 in	δ_2 in	$\frac{\delta_1}{\delta_2}$
3·950	measured	0·1715	0·0237	7·247
”	parabolic $r = 1$	0·1739	0·0212	8·195
”	parabolic $r = 0·89$	0·1722	0·0230	7·490

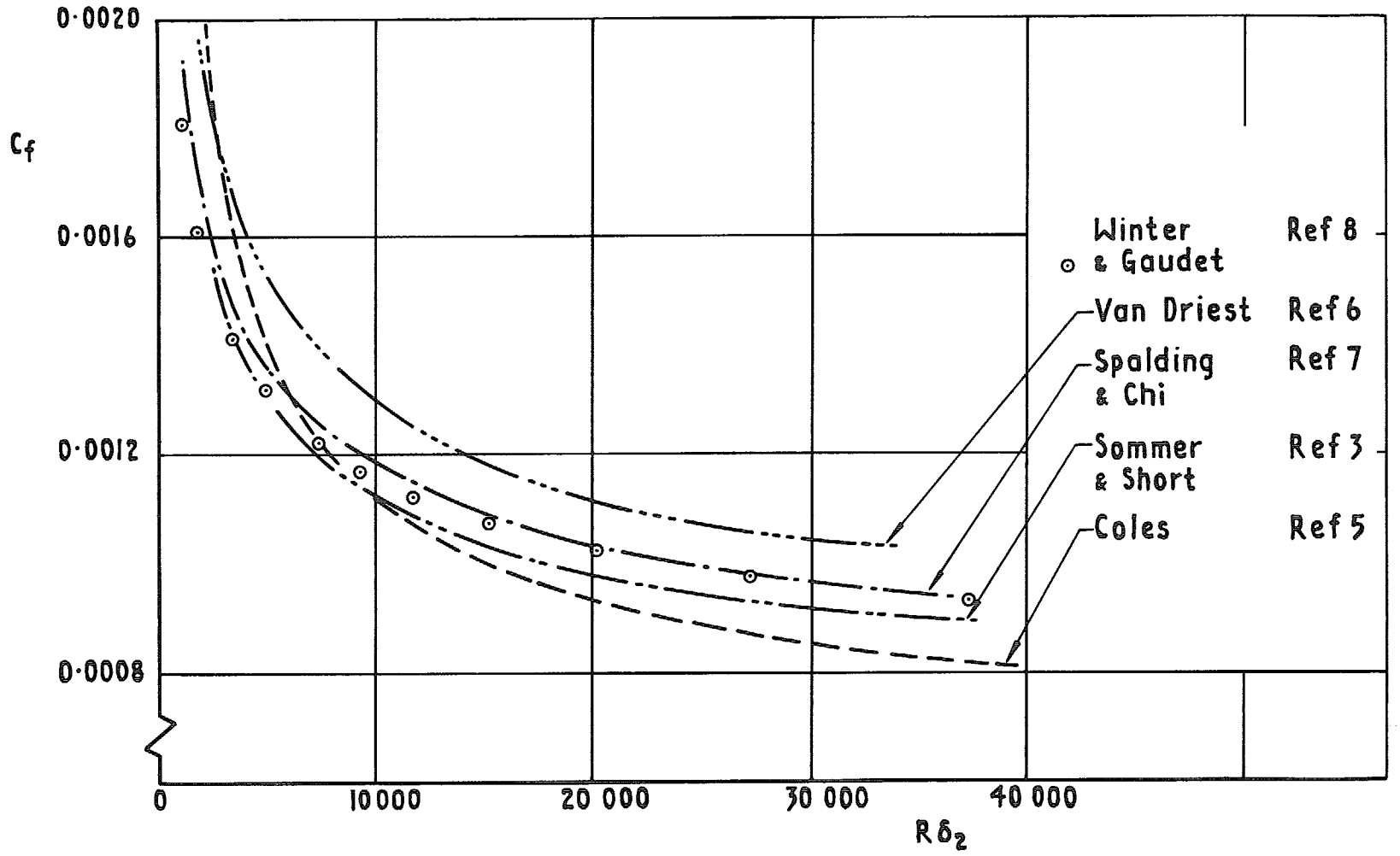

FIG. 1. Some theoretical skin friction laws for $M_e = 4$.

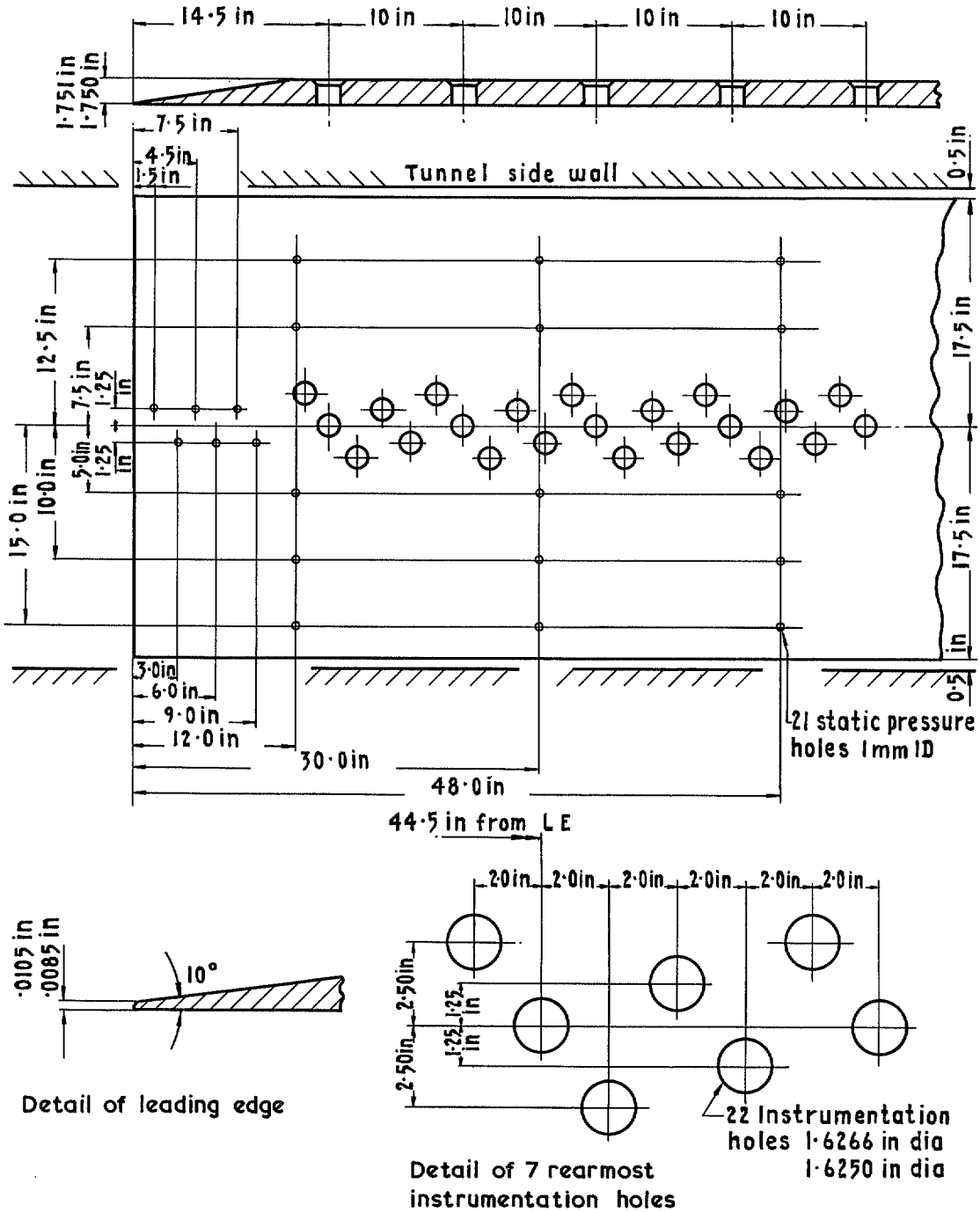

FIG. 2. Model details.

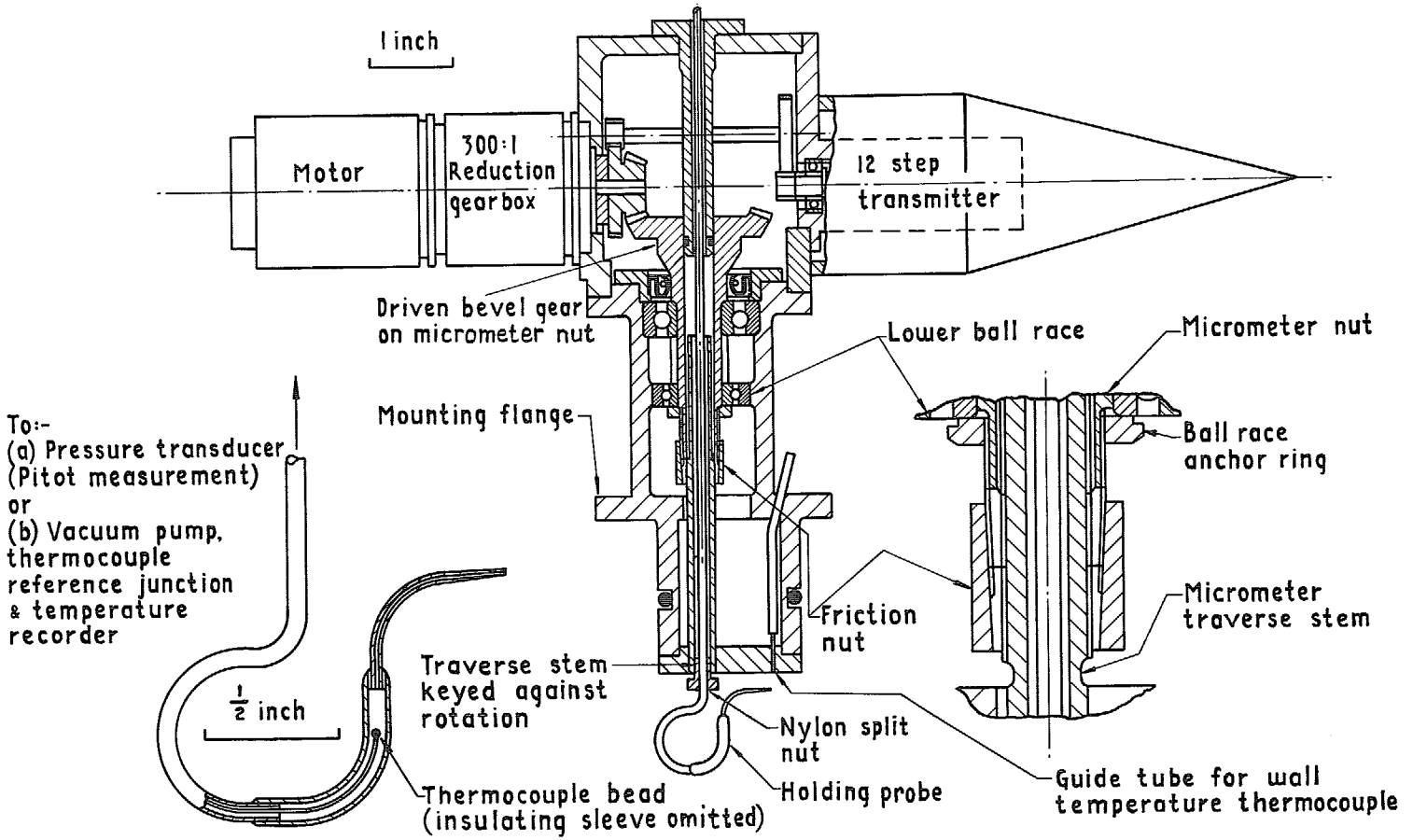

FIG. 3. Pitot traverse gear and probe.

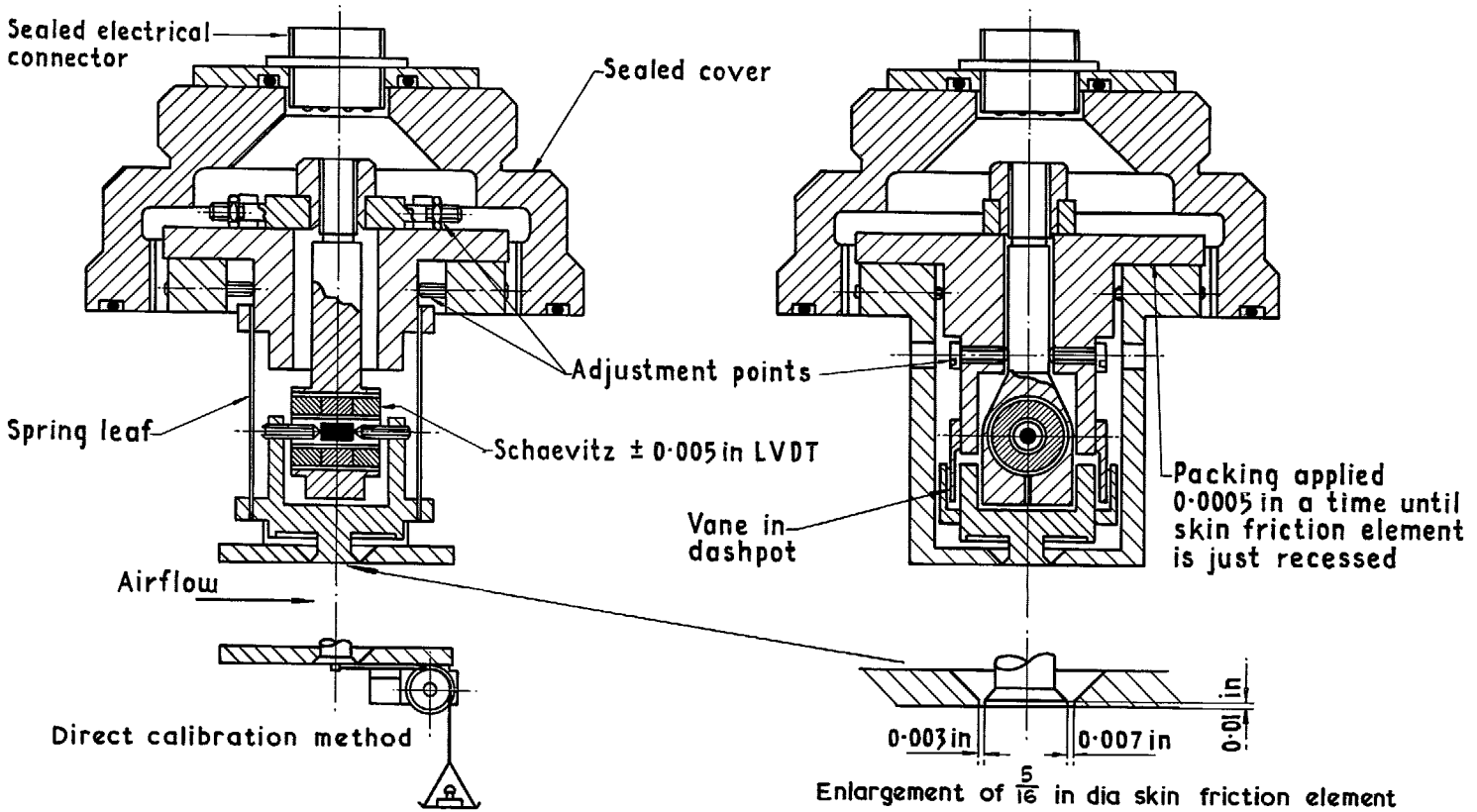

FIG. 4. Skin friction meter.

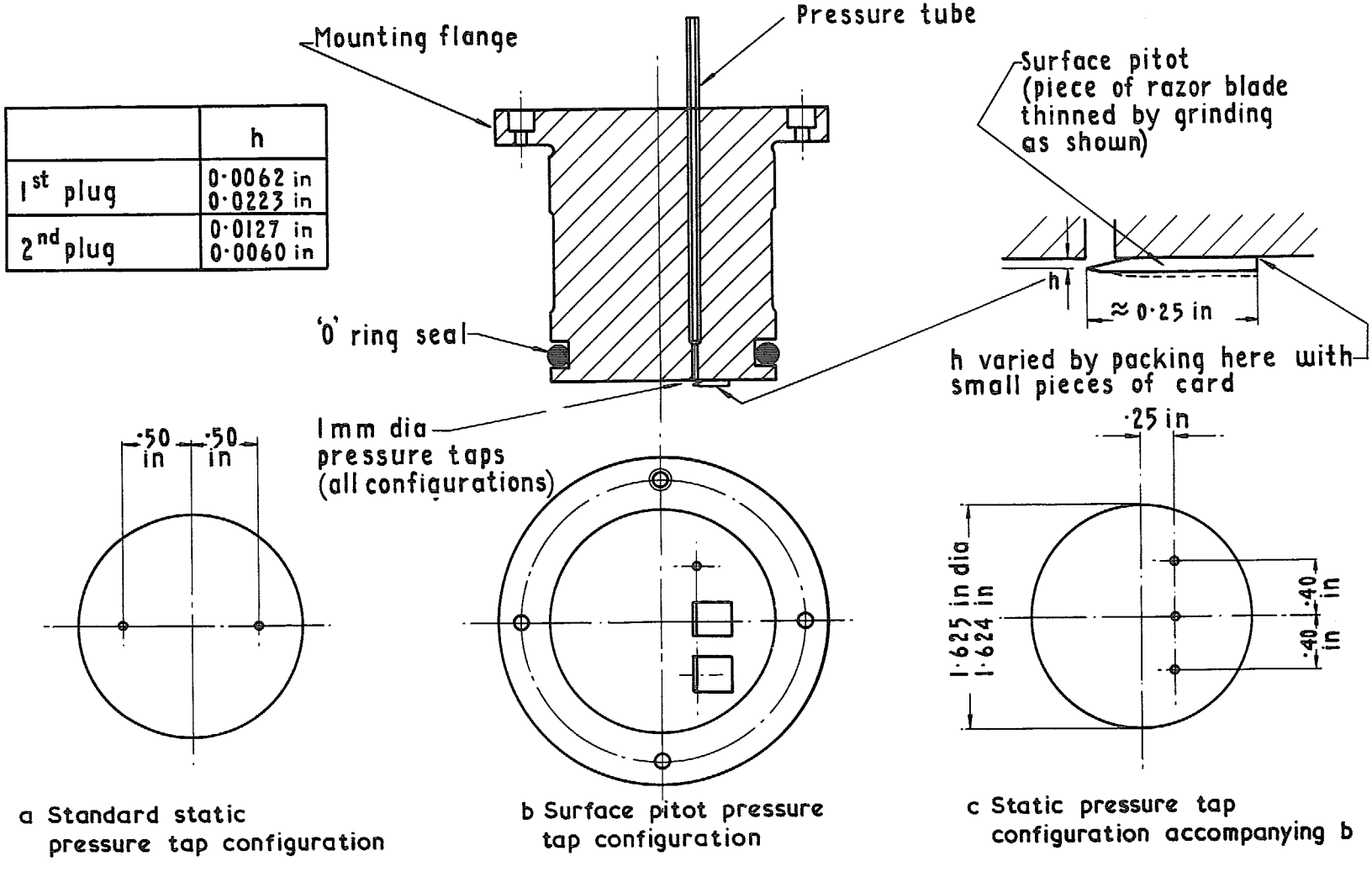

	h
1st plug	0·0062 in 0·0223 in
2nd plug	0·0127 in 0·0060 in

FIG. 5a–c. Pressure tapping plugs for flat plate model.

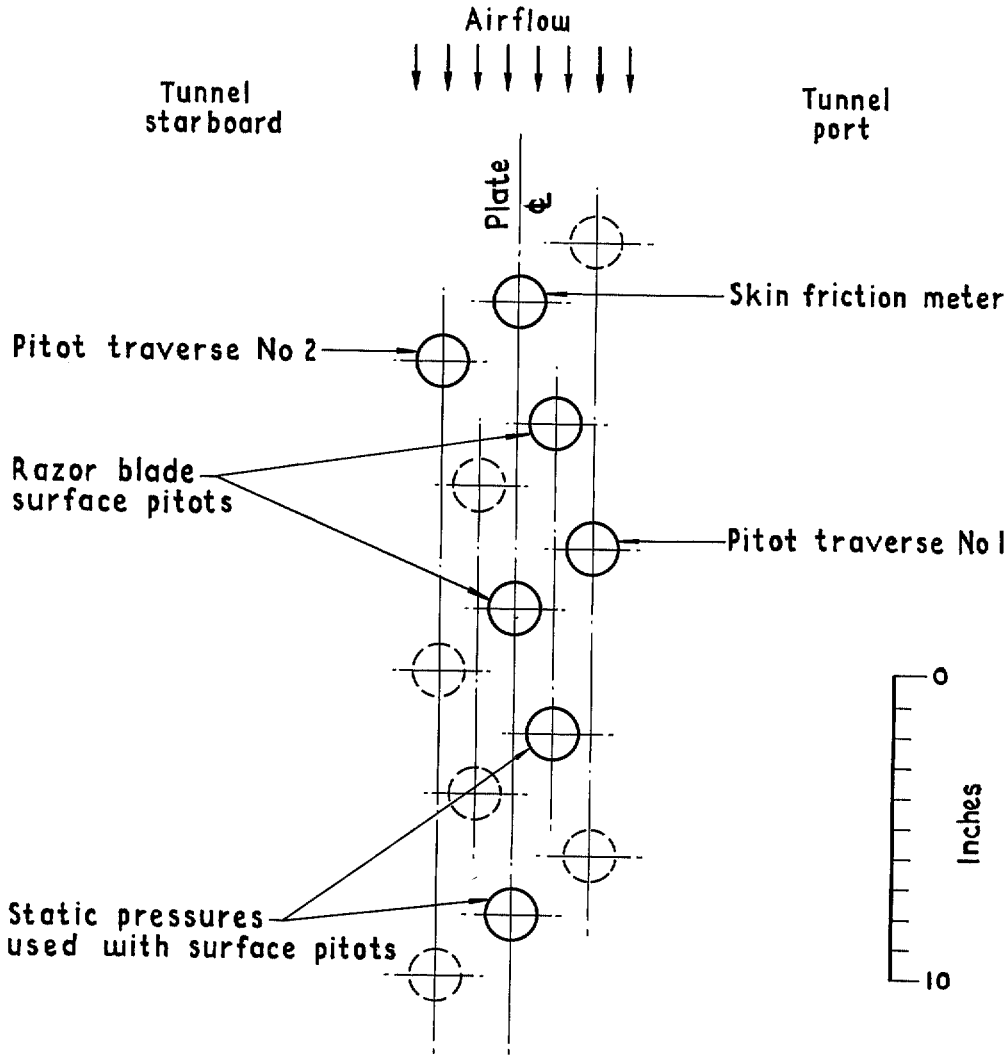

FIG. 6. Layout of standard instrumentation group as seen from below (working side).

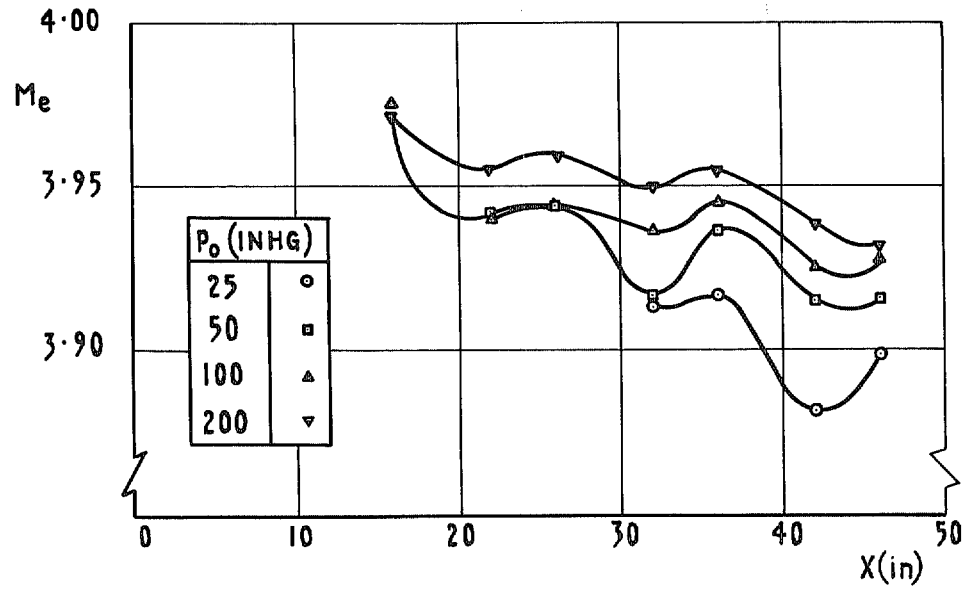

a Mach Number outside boundary layer

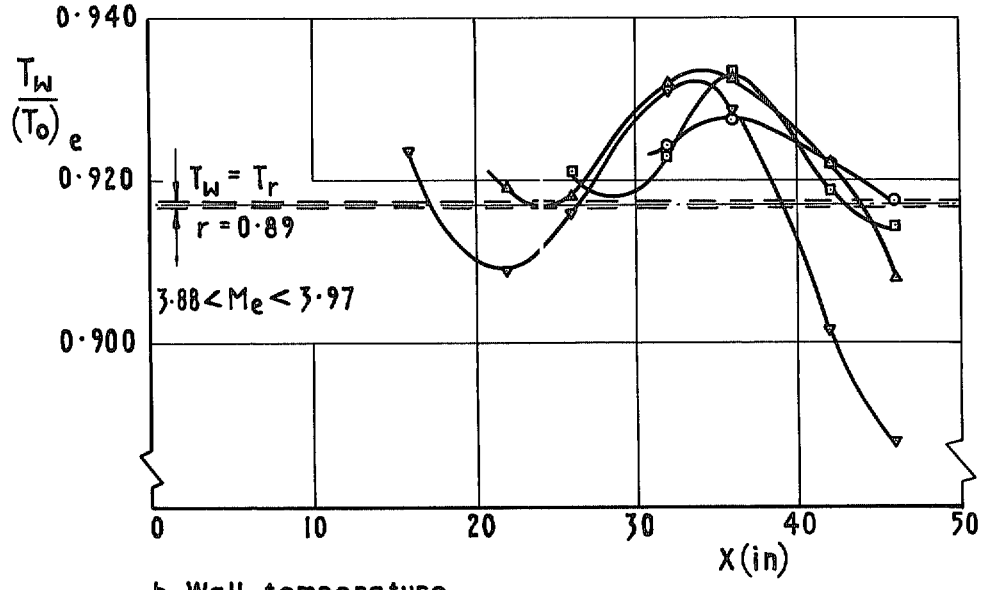

b Wall temperature

FIG. 7a & b. Flow conditions at traverse stations.

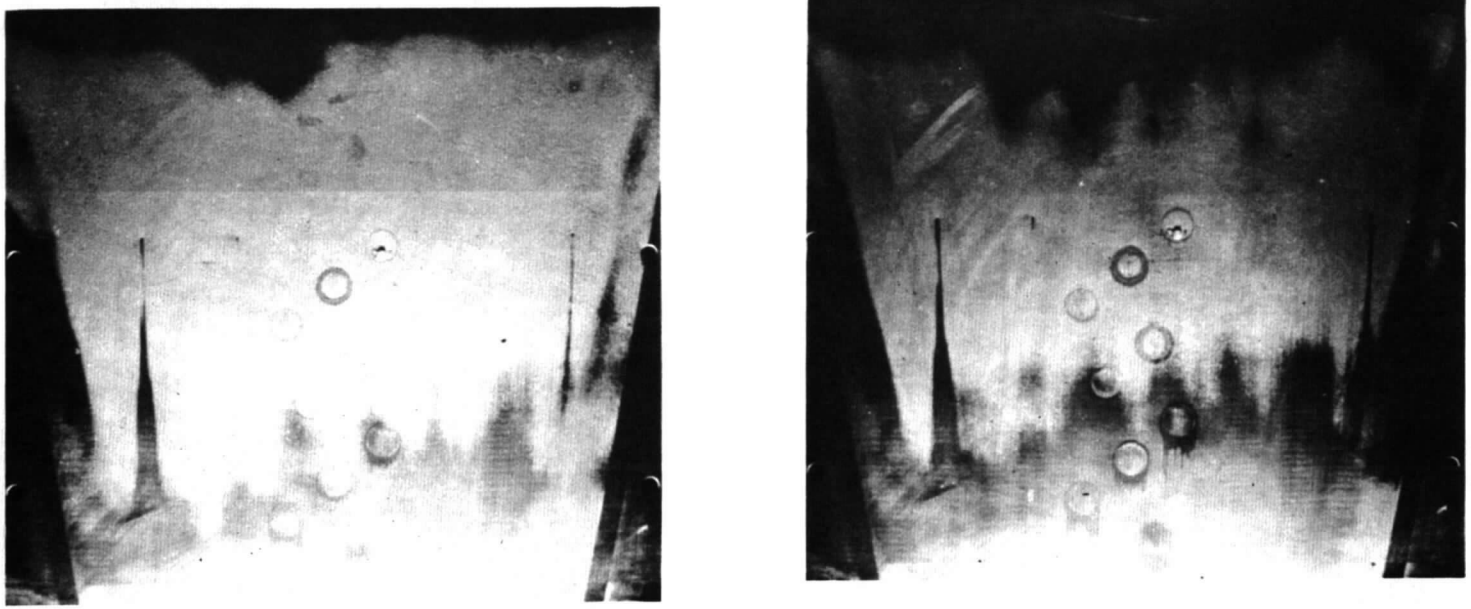

FIG. 8. Azobenzene transition patterns.

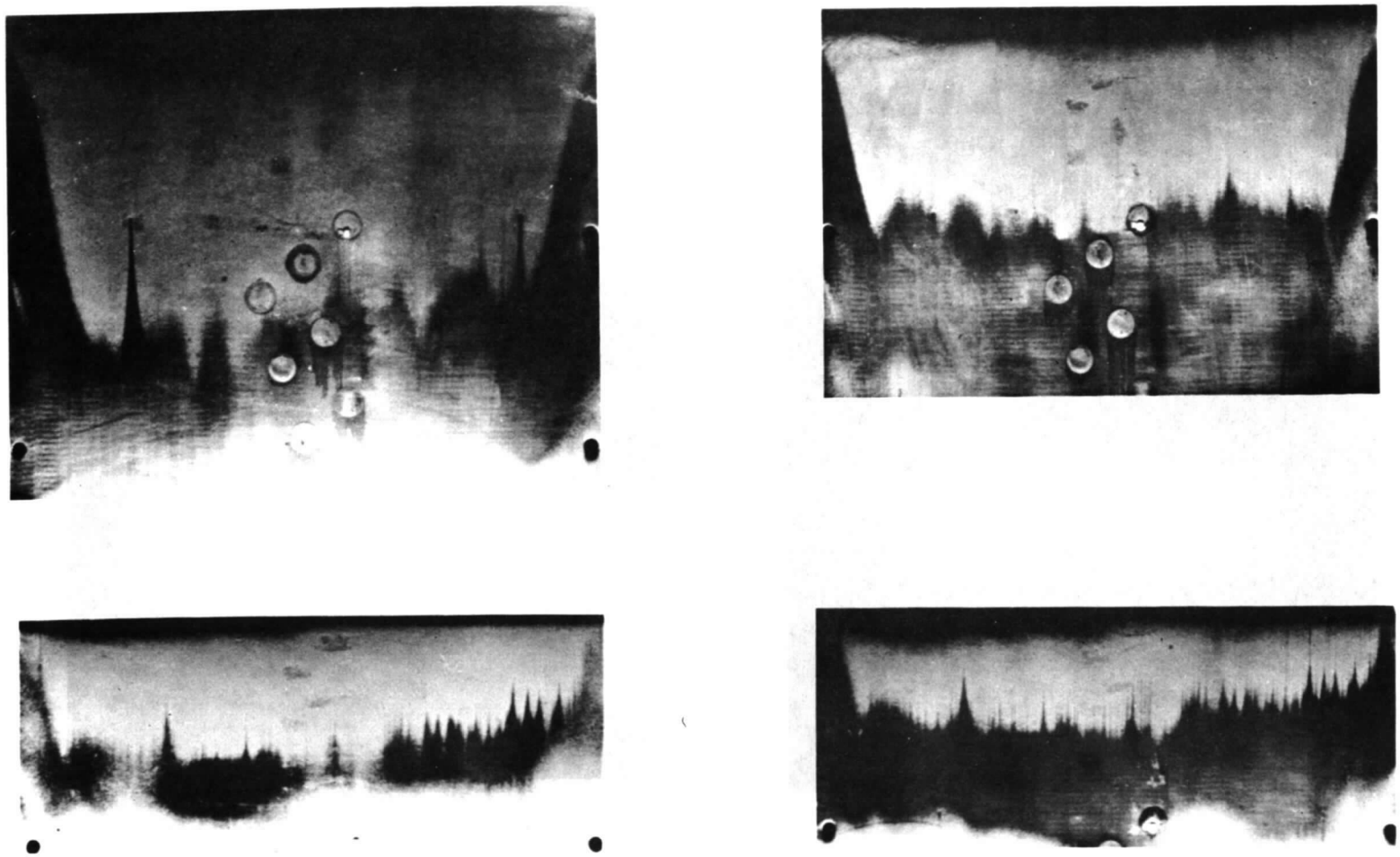

FIG. 8 (concl'd). Azobenzene transition patterns.

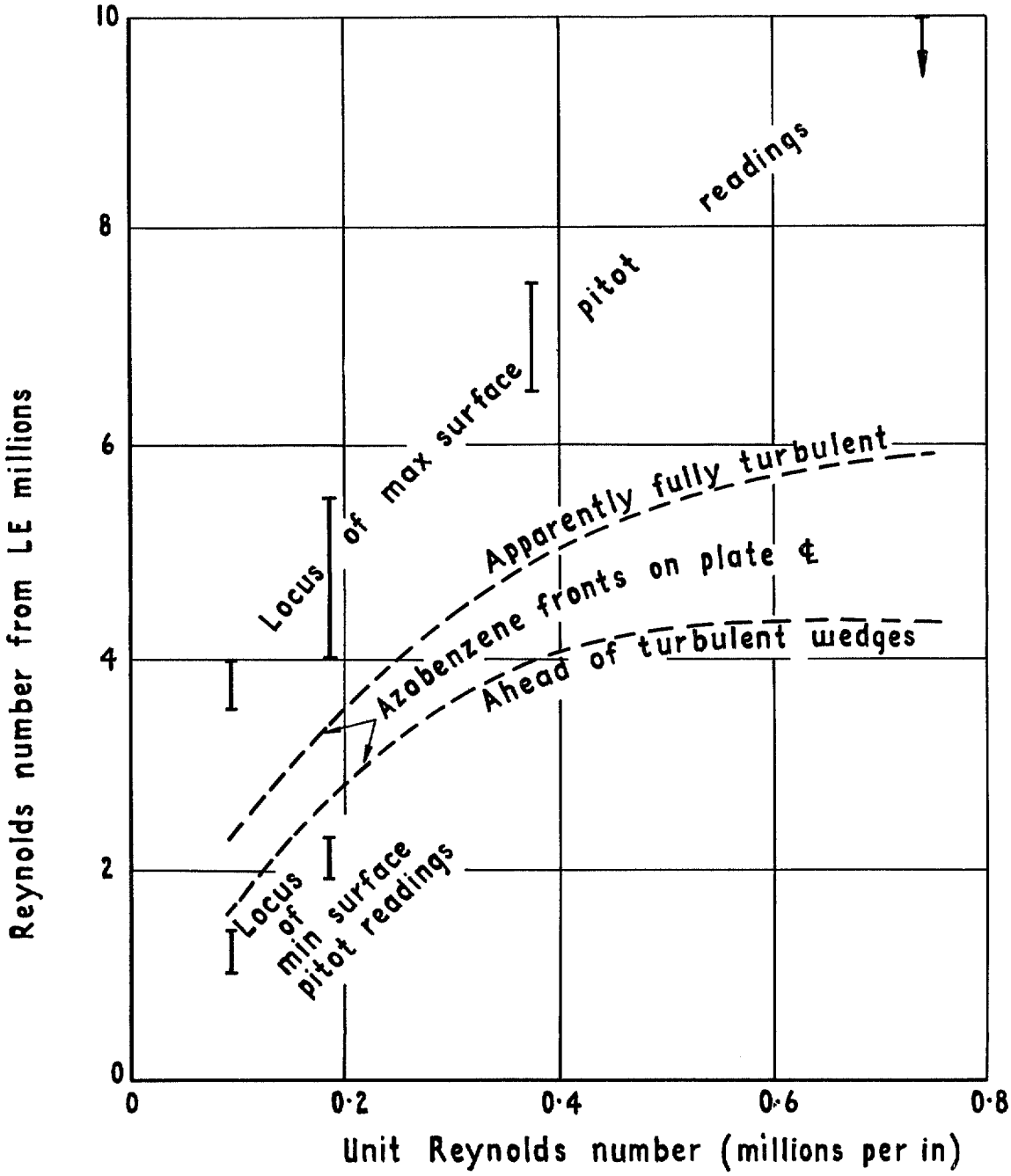

FIG. 9. Transition positions.

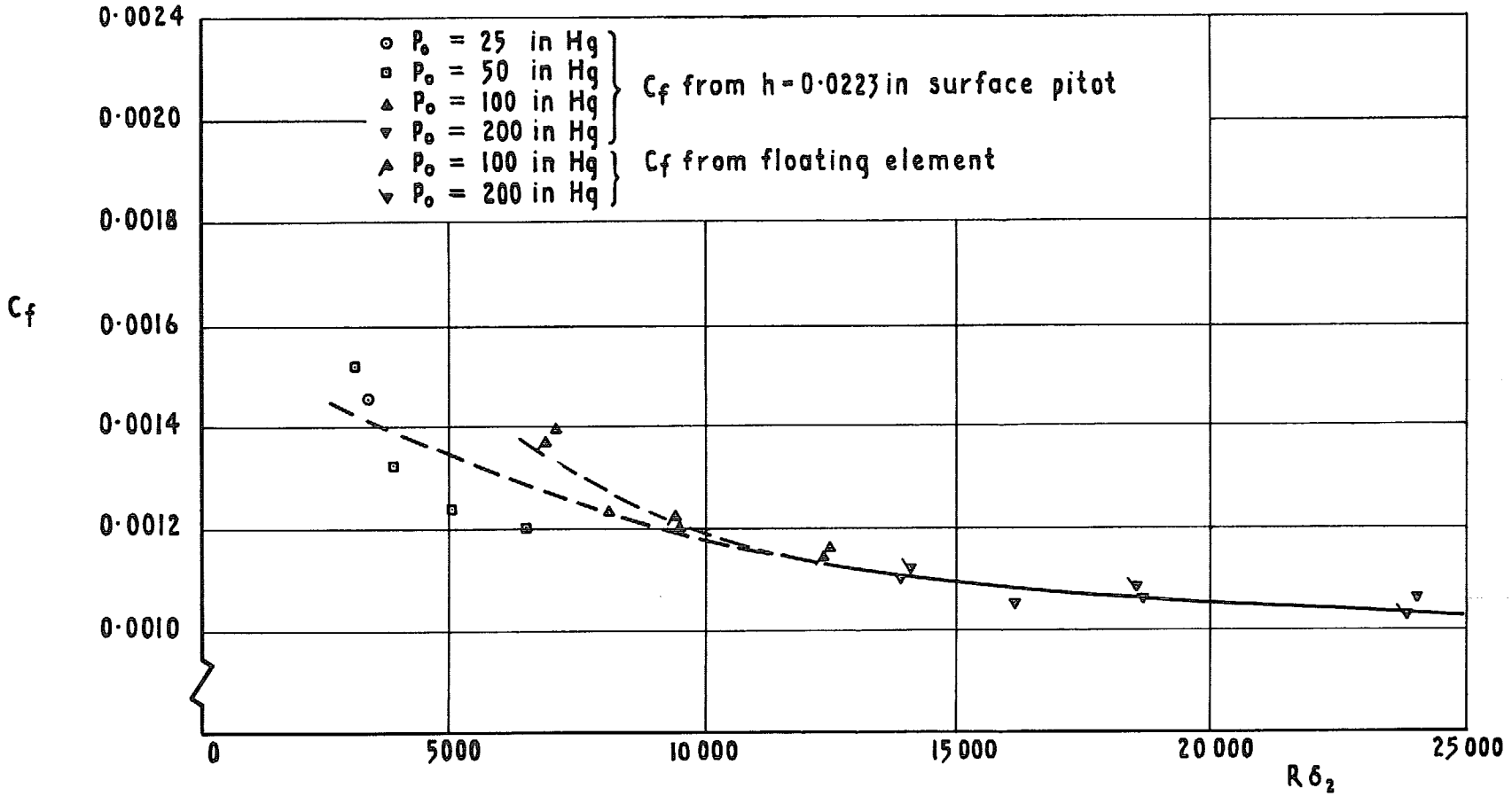

FIG. 10. Present skin friction data.

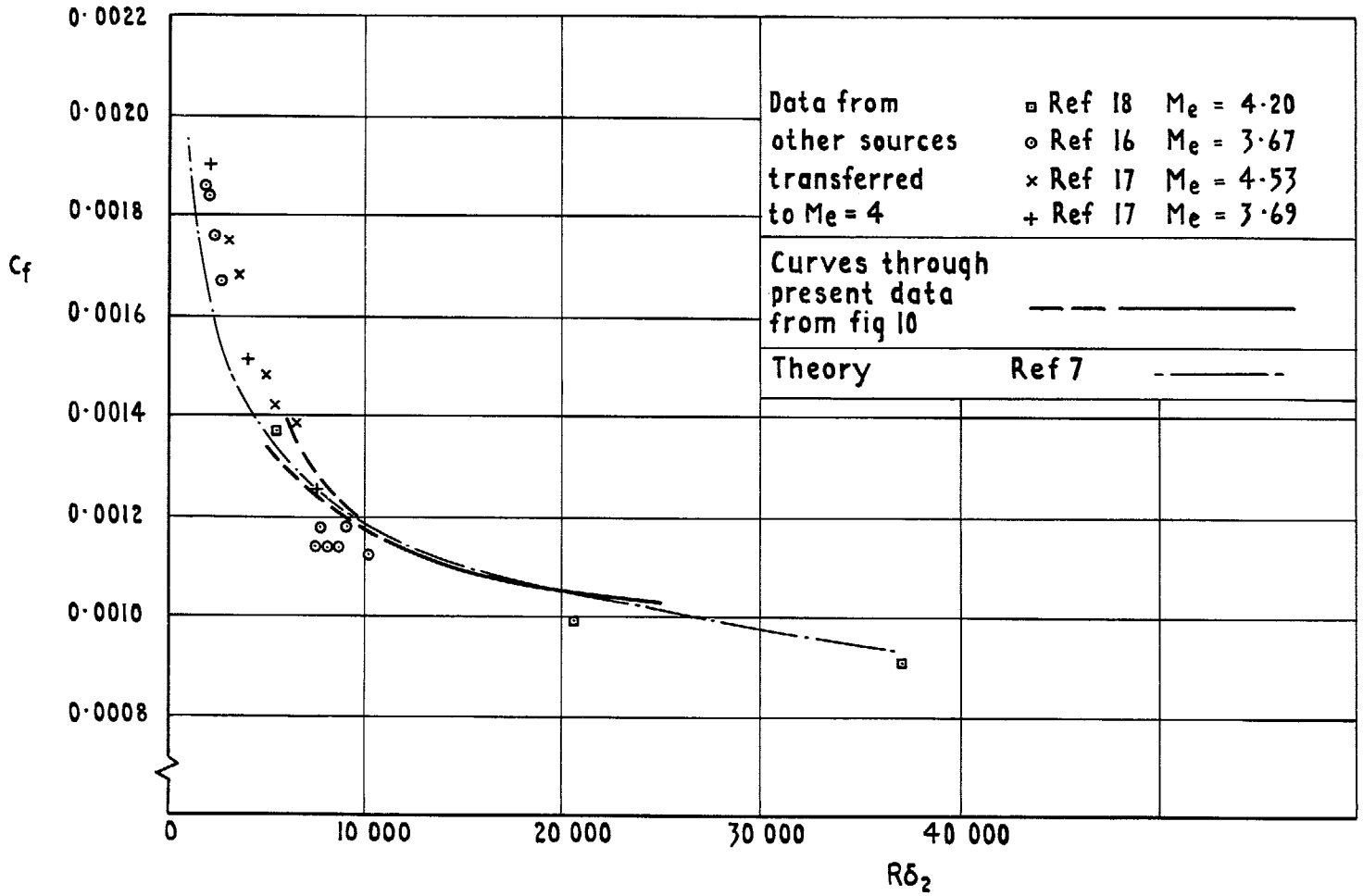

FIG. 11. Skin friction at $M_e = 4$ from present experiment and other sources.

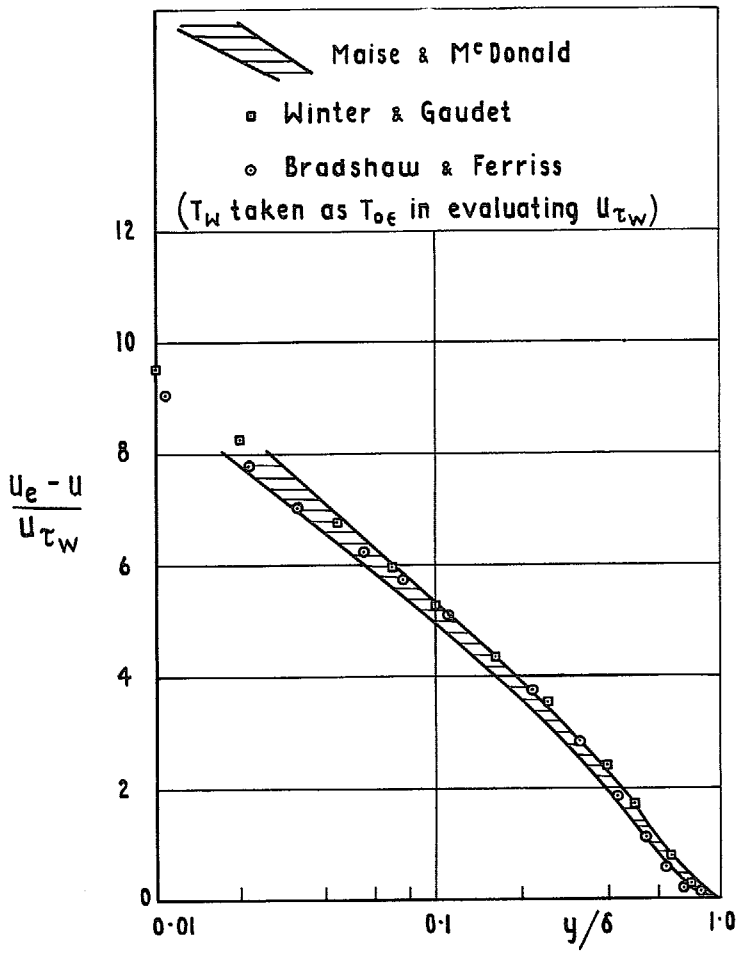

FIG. 12. Theoretical velocity-defect profiles at $M_e = 4$.

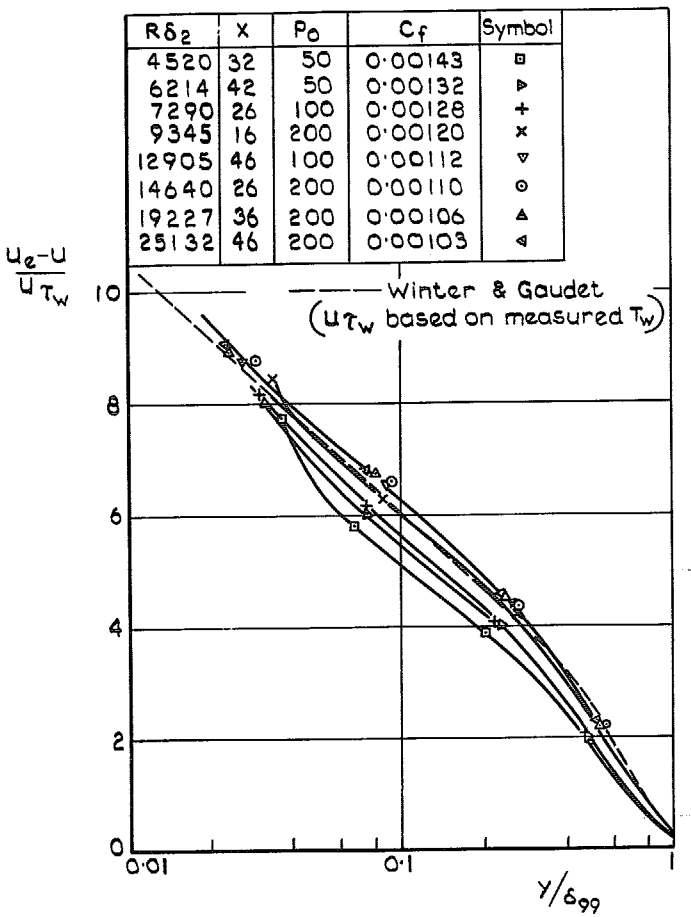

FIG. 13. Experimental velocity-defect profiles.

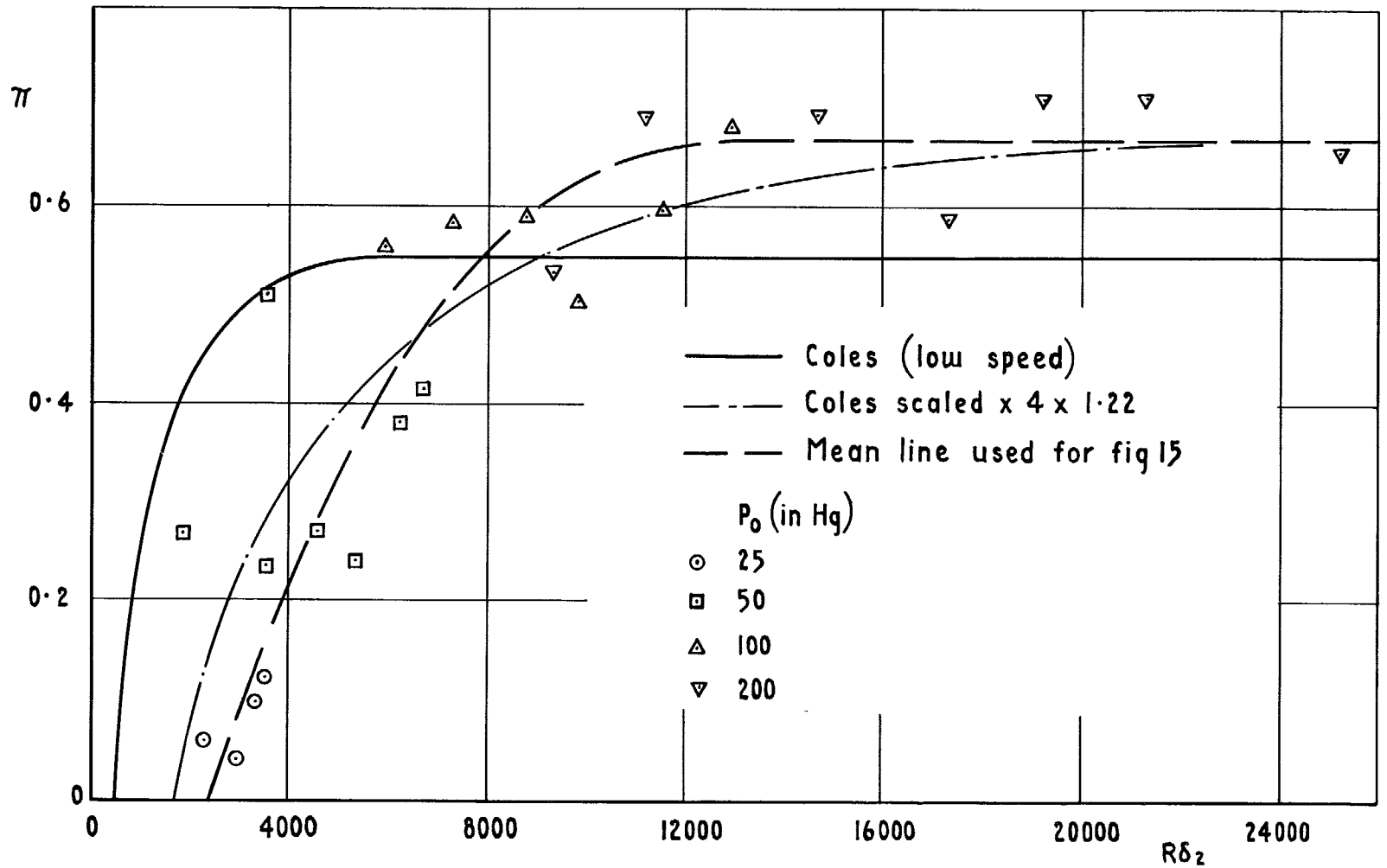

FIG. 14. Strength of wake component.

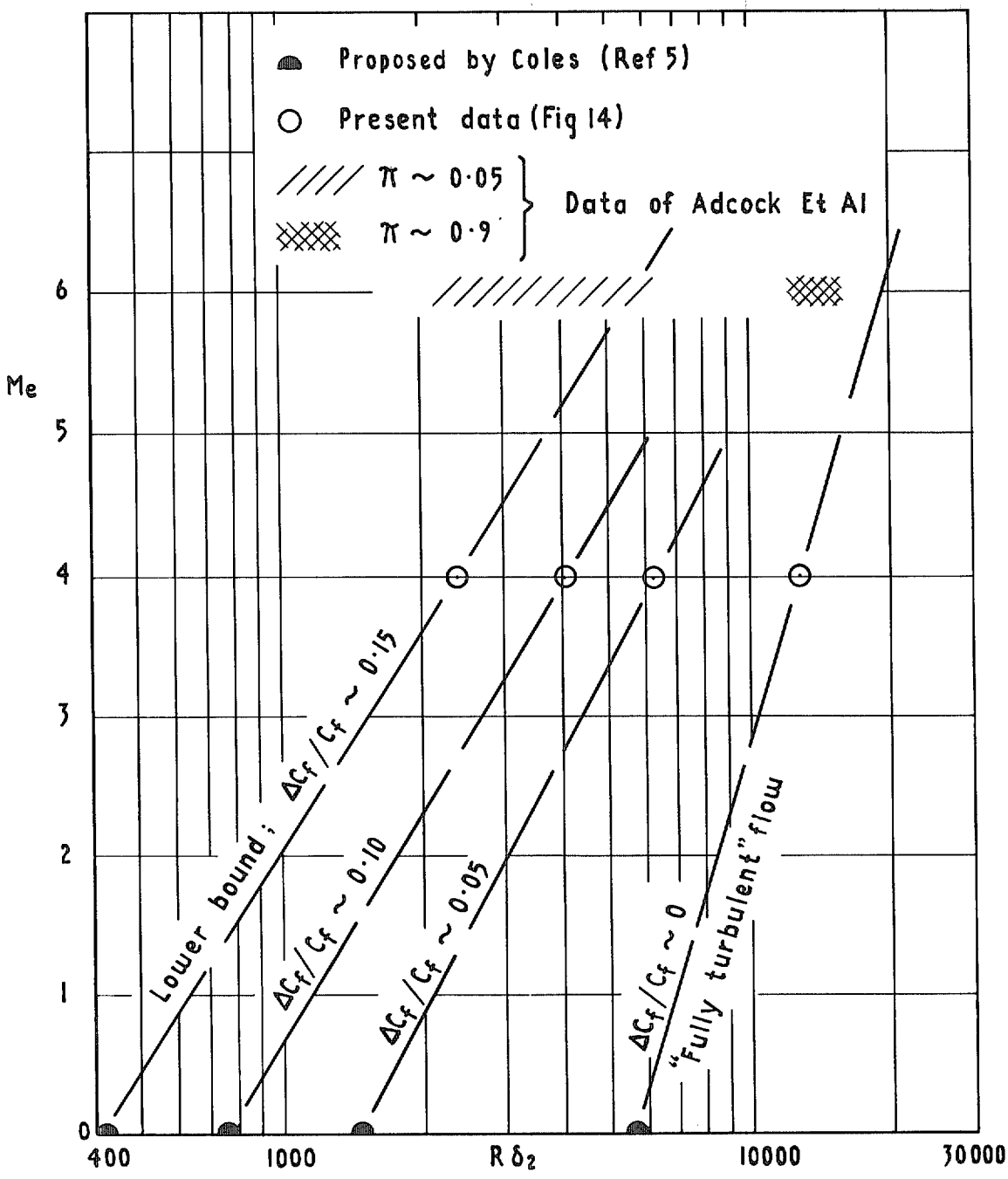

FIG. 15. Domain of divergence from 'fully turbulent' behaviour.

Printed in Wales for Her Majesty's Stationery Office by Allens Printers (Wales) Ltd.
Dd. 502110 K.5.

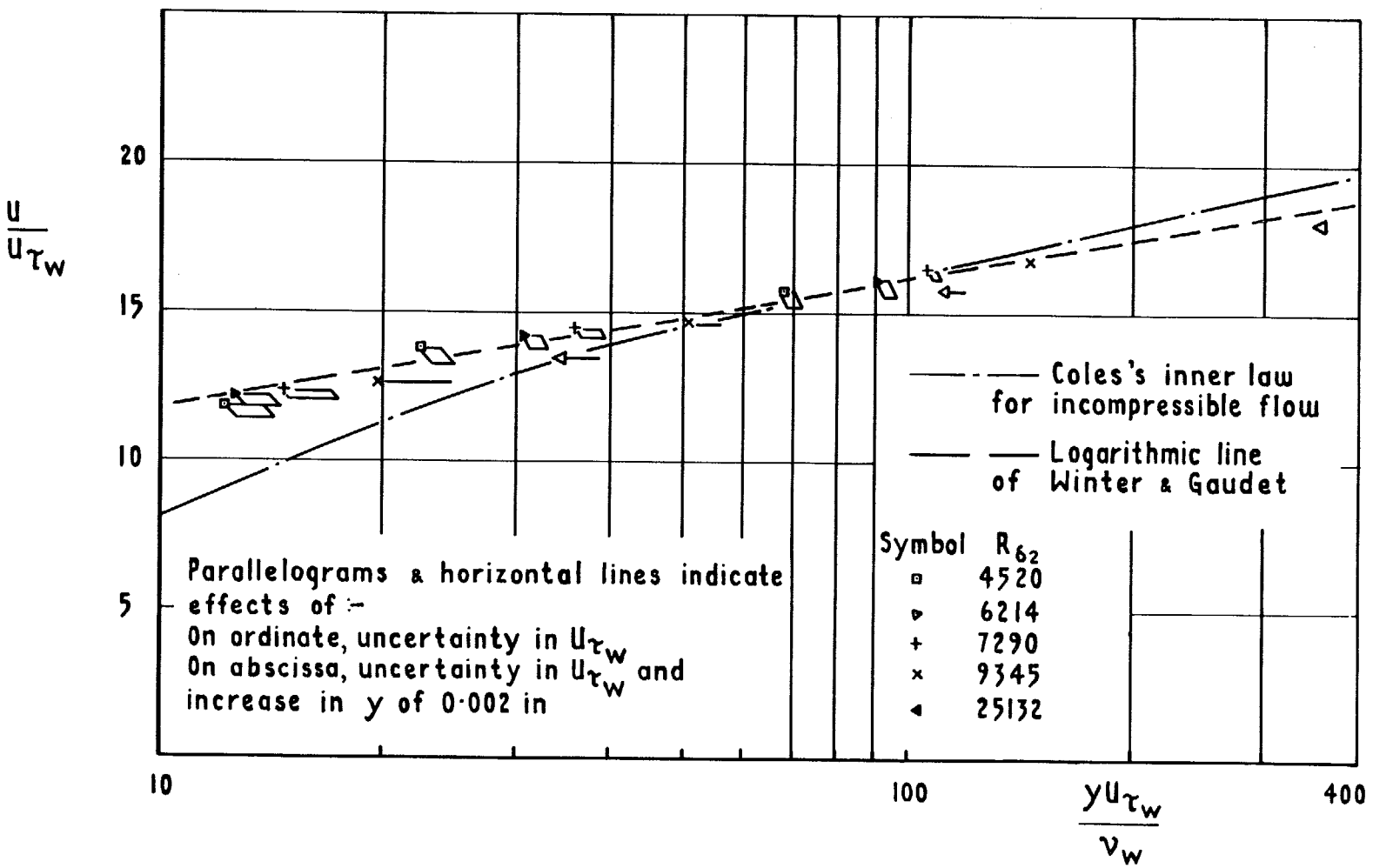

FIG. 16. Velocity profiles near the wall.

Published by
HER MAJESTY'S STATIONERY OFFICE

To be purchased from
49 High Holborn, London WC1V 6HB
13a Castle Street, Edinburgh EH2 3AR
109 St Mary Street, Cardiff CF1 1JW
Brazennose Street, Manchester M60 8AS
50 Fairfax Street, Bristol BS1 3DE
258 Broad Street, Birmingham B1 2HE
80 Chichester Street, Belfast BT1 4JY
or through booksellers

R. & M. No. 3678

SBN 11 470418 X